Integrated reduction and acid-catalysed conversion of furfural in alcohol medium using Zr,Al-containing ordered micro/mesoporous silicates

Margarida M. Antunes[a], Sérgio Lima[b], Patrícia Neves[a], Ana L. Magalhães[a], Enza Fazio[c], Fortunato Neri[c], Manuel T. Pereira[a], Carlos M. Silva[a], Silvia M. Rocha[d], Martyn Pillinger[a], Atsushi Urakawa[b], Anabela A. Valente[a,*]

[a] *CICECO - Aveiro Institute of Materials, Department of Chemistry, University of Aveiro, Campus Universitário de Santiago, 3810-193 Aveiro, Portugal*
[b] *Institute of Chemical Research of Catalonia, (ICIQ), Av. Països Catalans 16, 43007 Tarragona, Spain*
[c] *Dipartimento di Fisica e di Scienze della Terra, Università degli Studi di Messina, Viale F. Stagno d'Alcontres, 31 98166 Messina, Italy*
[d] *Department of Chemistry, QOPNA, University of Aveiro, Campus Universitário de Santiago, 3810-193 Aveiro, Portugal*

Abstract

Ordered porous silicates of the type TUD-1 and zeolite beta possessing zirconium and aluminium sites were evaluated as eco-friendly heterogeneous, multifunctional catalysts for the integrated reduction-acid conversion of furfural (Fur, industrially produced from hemicellulosic components of biomass) to useful bio-products, namely, furfuryl alcohol (FA), alkyl furfuryl ethers (FEs), alkyl levulinate esters (LEs), levulinic acid (LA), angelica lactones (AnLs), and γ-valerolactone (GVL); the bio-products spectrum was obtained by GC × GC-ToFMS. Carrying out the one-pot conversion of Fur to bio-products using a multifunctional catalyst is challenging since various reactions are involved and it is difficult to control all of these to meet high reaction efficiencies and selectivities. Aiming at designing improved multifunctional catalysts for this reaction system, the TUD-1 and zeolite beta type silicates possessing zirconium and aluminium sites in different ratios were prepared and characterised on microstructural and molecular levels. Systematic characterisation, catalytic testing using 2-butanol as dual functional solvent-H-donor, and kinetic modelling studies were performed using the Zr,Al-containing micro- and mesoporous materials. Different steps of the overall reaction of Fur were studied separately starting from intermediate products using the same materials, which helped understand the influence of the material properties on

reactivity of intermediates and reaction selectivity. Zr-sites of the silicate catalysts were essential for effectively initialising the overall process (reduction of Fur to FA), and for the reduction of LEs to GVL; the co-presence of Al-sites promoted acid-catalysed steps (FA to FEs, LEs, AnLs, LA). The good stability of the catalysts was verified by catalytic and characterisation studies of the spent catalysts.

1. Introduction

With the increasing worldwide demand for transportation fuels and consumer products, sustainability calls for sources of renewable chemical energy. In this context, plant biomass gains prominence as a renewable carbon source of chemicals and fuel additives since it is fairly wide-spread, can lead to emissions benefits (e.g. avoiding sulphur and global warming emissions associated with fossil fuels) and promote rural economic development. Lignocellulosic biomass is obtainable from forest/agricultural residues, municipal wastes (paper), and as by-products of the pulp and paper industry. The carbohydrate components of lignocellulosic biomass, mainly cellulose and hemicelluloses, can be converted to a plethora of useful intermediates for the chemical industry [1], [2], [3], [4], [5] and [6]. In particular, furfural (Fur) is a platform chemical, industrially produced from hemicelluloses (via acid-catalysed hydrolysis and dehydration), and its largest volume derivative is furfuryl alcohol (FA) [7], [8], [9] and [10], which is used for synthesizing less toxic resins for the foundry industry [8], [11] and [12]. Increasing the market penetration of Fur and FA, and expanding their applications profile can be beneficial for the bio-based economy. Besides FA, various useful bio-products, such as alkyl furfuryl ethers (FEs), levulinate esters (LEs), angelica lactones (AnLs), levulinic acid (LA), and γ-valerolactone (GVL) can be produced from Fur (Scheme 1) [13], [14] and [15]. For example, FEs are used as blending components of gasoline [16] and [17] and as flavours [18] and [19]. LEs are useful chemical intermediates for producing coatings, resins and flavour preparations [20] and [21], anti-cancer agents, pesticides and insecticides [22]. They are also used for removing nicotine, preserving fresh fruits [23], promising blend components in fuel formulations [20], [24], [25], [26] and [27] and green solvents [28]. AnLs are promising for preparing fuel additives [21] and [29], useful flavours and cigarette additives [30]. LA has been recognised as promising intermediate for producing fuel additives [31], [32], [33], [34], [35], [36] and [37], agrochemicals [36] and [38] and polymers [36] and [39]. GVL is an attractive green solvent [40], [41] and [42] and is of value in the fuels sector [32], [43], [44], [45] and [46].
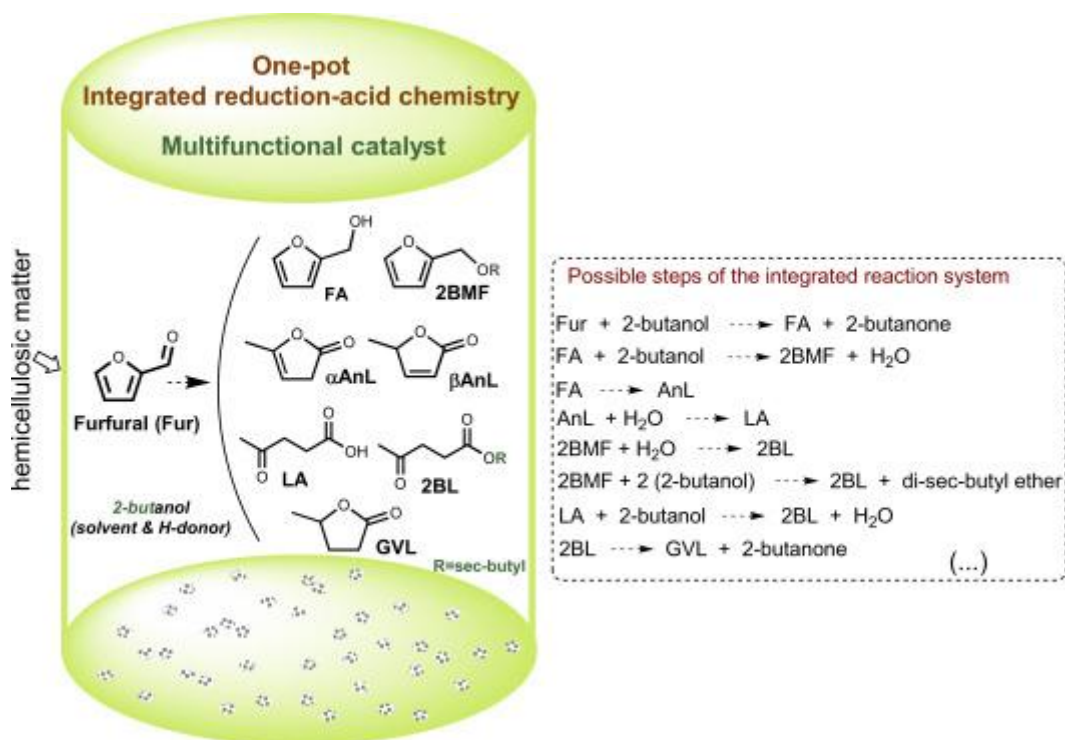
Scheme 1. Simplified representation of the conversion of Fur (derived from hemicellulosic matter) to useful bio-products, and the challenging approach of integrating the reductions and acid reactions involved, in one-pot using a multifunctional catalyst; possible (balanced) stoichiometric chemical equations for some reactions (on the right).

Strategies for the valorisation of bio-based chemicals via integrated catalytic reaction systems (one-pot synthesis) have been investigated because of their importance in the context of sustainable chemical processes [47]. There are difficult challenges which have to be overcome, such as controlling various chemical reactions in one operation, and obtaining high reaction selectivity. The synthesis of bio-products from Fur involves complex reductions and acid chemistry. Different acid-catalysed routes leading to bio-products in alcohol/aqueous media have been reported in the literature, specifically: (i) FA to FEs [48]; (ii) FA to LEs [49] and [50] via intermediate formation of FEs [51], [52], [53], [54] and [55], 4,5,5-trialkoxypentan-2-one intermediates [52] or AnLs [51] and [56], or FA to LA via the intermediate 4,5,5-trihydroxypentan-2-one [57]; (iii) LA [23] and [50] and αAnL to LEs [46] and [58]; (iv) FA [51] and [56] and LA to AnLs [36]; (v) Fur/FA [16] and [59] or αAnL [60] to LA. On the other hand, Fur and intermediate bio-products can be reduced via a catalytic transfer hydrogenation (CTH) reaction with a H-donor agent (e.g. aliphatic alcohol), specifically: (i) Fur to FA [61] and [62] and/or FEs [63] and [64]; (ii) LEs [20], [62], [65], [66], [67] and [68], AnLs [36] and [69] or LA [67] and [70] to GVL. The use of an aliphatic alcohol solvent for Fur conversion has been reported to enable more direct synthesis routes leading to bio-products such as FEs and LEs [52], at the same time, avoiding formation of process chemicals such as humins (commonly occurring in aqueous phase processes) which can deposit and lead to technical problems. Moreover, the alcohol solvent may simultaneously act as H-donor for CTH reactions, which presents several advantages compared to high-pressure H_2 catalytic reduction systems, such as relatively mild reaction conditions and no need for expensive and leachable noble metal catalysts. In the context of green chemistry, the catalysts should be preferably heterogeneous, have eco-friendly compositions and possess good stabilities. Furthermore, integrated (one-

3

pot) catalytic reaction system using one multifunctional catalyst is very attractive in terms of process intensification, instead of multiple synthesis processes using monofunctional catalysts.

Porous mixed oxides based on silicon, aluminium and zirconium can be eco-friendly and robust multifunctional catalysts for integrated reduction-acid catalytic systems, since Al-sites may promote the acid chemistry, while Zr-sites the reduction chemistry via the above mentioned CTH approach. For example, zirconium alkoxide grafted onto mesoporous silica promoted CTH reactions of aliphatic alcohols (e.g. geraniol) with Fur; when zirconium species were grafted onto an acidic aluminosilicate support (Al-MCM-41) the obtained material acted as a multifunctional catalyst promoting acid-catalysed steps (e.g. dehydration, isomerisation) besides CTH ones [71]. In different studies, it was demonstrated that Zr-containing zeolite beta (Zr-silicate) selectively promoted CTH reactions in alcohol medium, such as LA [70] and LEs [65] to GVL. More recently, it was reported that Zr-beta mechanically mixed with H-beta promoted the conversion of Fur to GVL [63]. These results motivated us to investigate Zr,Al-containing porous silicates as multifunctional catalysts for the one-pot conversion of Fur to bio-products.

In this work, we focused on ordered meso- and microporous silicates possessing Al- and/or Zr-sites with different Al/Zr ratios for the one-pot conversion of Fur to bio-products, using 2-butanol with the dual function of solvent and H-donor at 120 °C. Specifically, TUD-1 type ordered mesoporous materials were prepared via non-surfactant templating methods with benefits in terms of decreased toxicity and costs [72], [73], [74], [75] and [76]. In addition, microporous zeotype materials possessing the BEA topology were prepared by post-synthesis dealumination of commercial nanocrystalline zeolite H-beta, and subsequent solid-state ion-exchange (SSIE) for Zr or (Zr + Al). This synthesis methodology is speedy compared to conventional hydrothermal synthesis, up-scalable and does not destroy the zeolitic framework [77], [78], [79] and [80]. Characterisation and catalytic studies of the Zr- and Al-containing materials were systematically combined to help understand the influence of material properties on the different steps of the overall reaction process. The reaction products were identified by comprehensive two-dimensional gas chromatography (GC × GC) combined with time-of-flight mass spectrometry (ToFMS). Mechanistic and kinetic modelling studies helped establish relationships between material properties and catalytic performances for different reaction steps. Catalyst stability was evaluated by catalytic and characterisation studies of the spent catalysts.

2. Experimental

2.1. Synthesis of the catalysts

2.1.1. Chemicals and materials

Zirconium(IV) acetylacetonate (98%, Sigma–Aldrich), zirconium(IV) propoxide (70 wt.% in 1-propanol, Aldrich), aluminium acetylacetonate (99%, Sigma–Aldrich), aluminum(III) isopropoxide (>98%, Alfa Aesar), tetraethyl orthosilicate (TEOS: 98%, Aldrich, for beta type materials; ≥99.0%, Sigma–Aldrich, for TUD-1 type materials), triethanolamine (TEA; 97%, ACROS), ethanolamine (≥99.0%, Sigma–Aldrich), tetraethylammonium hydroxide solution (TEAOH; 35 wt.% in water, Aldrich), 2-

propanol (99%, Aldrich, for beta type materials; >99.5% Alfa Aesar/CYMIT, ACS, for TUD-1 type materials), ethanol (VWR, >99.8% ACS, ISO, AnalaR NORMAPUR), 2-butanol (99%, Sigma–Aldrich), furfural (Fur, 99%, Aldrich), furfuryl alcohol (FA; 99%, Aldrich), 1-butyl levulinate (1BL; 98%, Aldrich), α-angelica lactone (α-AnL; 98%, Alfa Aesar), levulinic acid (LA; 98%, Aldrich), and ethyl furfuryl ether (EMF; 97%, Manchester Organics) were used as received. The water was MiliQ. The Al- and Zr-containing beta materials were prepared from commercial nanocrystalline NH_4-beta (Zeolyst, CP814E; 20-30 nm crystallites).

2.1.2. Beta type materials

The Zr- and Al-containing beta materials were prepared from nanocrystalline NH_4-beta, following similar protocols to those described in the literature [46] and [78], which involved (i) calcination of NH_4-beta (550 °C, 10 h) to give H-beta, (ii) partial dealumination of H-beta with HNO_3 (13 M aq., 100 °C) to give deAl-beta (possessing a framework with vacant tetrahedral sites), (iii) solid-state ion-exchange (SSIE) to introduce the desired metal centers into the framework, and (iv) final calcination at 550 °C in an air flow (20 mL min^{-1}) for 3 h. The H-beta and deAl-beta (prepared by treating H-beta with 13 M aq. HNO_3) samples were the same as those reported in ref. [46]. The material deAl-beta was subjected to SSIE for Zr, or Zr plus Al giving (Zr)$_{SSIE}$-beta and (ZrAl)$_{SSIE}$-beta, respectively. For (Zr)$_{SSIE}$-beta, a solid mixture of zirconium(IV) acetylacetonate and deAl-beta (0.844 mmol Zr per gram of deAl-beta) was ground in an agate pestle and mortar at room temperature. The material (ZrAl)$_{SSIE}$-beta was prepared in a similar fashion to (Zr)$_{SSIE}$-beta, but using equimolar amounts of zirconium(IV) acetylacetonate and aluminium acetylacetonate; 0.844 mmol (Zr + Al) per gram of deAl-beta. Finally, the solid mixtures were subjected to calcination at 550 °C (heating rate of 1 °C min^{-1}) under air flow (20 mL min^{-1}) for 4 h. For comparative studies, bulk ZrO_2 was prepared via thermal treatment of zirconium(IV) acetylacetonate using the same calcination conditions as those used for the Zr-containing beta materials.

2.1.3. TUD-1 type materials

The TUD-1 type materials were synthesised by the sol–gel method, using TEA as templating agent. Al-TUD-1 was synthesised using identical conditions to those described in Ref. [81], and the Zr-containing TUD-1 materials were synthesised in a similar fashion to that described in the literature [82] and [83]. Specifically, Zr-TUD-1 was synthesised using TEOS and zirconium(IV) propoxide as Si- and Zr-sources, in a molar ratio Si/Zr of ca. 18. TEOS (16.9 g) was added to a mixture of zirconium(IV) propoxide (1.49 g) and 2-propanol (12.5 mL). After stirring for 10 min, a mixture of TEA (12.25 g) and water (9.25 mL) was added with vigorous stirring for 1 h until a gel was obtained, followed by addition of TEAOH solution (10.05 g) with vigorous stirring.

Two samples of (Zr,Al)-containing TUD-1 were synthesised under similar conditions, keeping constant the molar ratio Si/(Al + Zr) (ca. 21) of the synthesis gel, but changing the molar ratio Al/Zr, giving the materials (ZrAl)-TUD-1(x) (x was ca. 0.7 or 0.3). For (ZrAl)-TUD-1(0.7), aluminum(III) isopropoxide (0.34 g) and zirconium(IV) propoxide solution (0.745 g) were first added to a 1:1 (v/v) mixture of 2-propanol (6.5 mL) and ethanol (6.5 mL), and stirred at room temperature until complete dissolution. The obtained solution was added to TEOS (17.3 g) while vigorously stirring for 10 min.

Then, a mixture of ethanolamine (12.5 g) and water (9.4 g) was added and kept under vigorous stirring for at least 2 h until a gel was obtained, followed by addition of TEAOH (10.2 g) under vigorous stirring. The synthesis conditions for (ZrAl)-TUD-1(0.3) were the same as those for (ZrAl)-TUD-1(0.7), except that the molar ratio Al/Zr of the synthesis gel was 0.3.

For each material, the corresponding synthesis gel was aged under static conditions (at room temperature for 24 h) and then dried at 98 °C for 24 h. The obtained solids were gently ground, and then transferred into a Teflon-lined autoclave, followed by hydrothermal treatment at 180 °C for 8 h. Finally, the solids were calcined at 600 °C (heating rate of 1 °C min^{-1}) for 10 h in air.

2.2. Characterisation of the catalysts

The wide-angle powder X-ray diffraction (PXRD) patterns ($10° < 2\theta < 70°$) were recorded on a D8 Advance Series 2 Theta/Theta powder diffraction system (Bruker) with Cu-Kα radiation and step size of 0.02°. The low-angle powder XRD patterns ($1 < 2\theta/° < 10$) were recorded on a Siemens EM-10110BU model D5000 Theta/Theta powder diffraction system (Bruker) with CuKα radiation, and step size of 0.01°. Scanning electron microscopy (SEM) images, energy dispersive X-ray spectroscopy (EDS) analysis and elemental (Zr, Al and Si) mappings were obtained on a Hitachi SU-70 SEM microscope with a Bruker Quantax 400 detector operating at 20 kV.

ICP-AES measurements were carried out using an ICP-OES Horiba Jobin Yvon spectrometer, model Activa M. The thermogravimetric analyses (TGA) and differential scanning calorimetry (DSC) analyses were carried out under air with a heating rate of 10 °C min^{-1}, using Shimadzu TGA-50 and DSC-50 instruments, respectively. Nitrogen adsorption–desorption isotherms were measured at −196 °C on an Autosorb-iQ (Quantochrome Instruments). Prior to measurements, the solids were out-gassed at 300 °C for 12 h, under vacuum using a Pfeiffer HiPace 80 turbomolecular pump. The following textural properties of the materials were determined from the N$_2$ adsorption isotherms: specific surface area (S$_{BET}$) using the Brunauer–Emmett–Teller (BET) equation, total pore volume at relative pressure (p/p_0) of ca. 0.98, and external surface area (S$_{ext}$) and micropore volume (V$_{micro}$) using the t-plot method. The mesopore size distribution (MSD) curves of the TUD-1 type materials were calculated from the corresponding desorption branches using the BJH method; the median of the MSD curve was used to compare pore widths of different materials.

Fourier transform infrared (FT-IR) spectra were recorded in transmission mode as KBr pellets using a Unican Mattson Mod 7000 spectrophotometer equipped with a DTGS CsI detector (400–4000 cm^{-1}, 256 scans, 4 cm^{-1} resolution). Diffuse reflectance UV–vis spectra were recorded using a Jasco V-560 spectrophotometer and BaSO$_4$ as reference. The ^{27}Al MAS NMR spectra of (Zr)$_{SSIE}$-beta were recorded at 182.432 MHz using a Bruker Avance III HD 700 (16.4 T) spectrometer with a unique pulse, a recycle delay of 1 s, and a spinning rate of 14 kHz. For the remaining materials ((ZrAl)$_{SSIE}$-beta, (ZrAl)-TUD-1(x) and Al-TUD-1) the ^{27}Al MAS NMR spectra were recorded at 104.26 MHz using a Bruker Avance 400 (9.4 T) spectrometer with a contact time of 3 ms, a recycle delay of 1 s, and a spinning rate of 13 kHz. Chemical shifts are quoted in ppm from Al(NO$_3$)$_3$. X-ray photoelectron spectroscopy (XPS) analysis was performed on a K-alpha system from Thermo Scientific, equipped with a monochromatic Al Kα source

(1486.6 eV), and operating in constant analyser energy (CAE) mode with a pass energy of 200 and 50 eV for survey and high resolution spectra, respectively. A spot size diameter of about 400 μm was adopted, which is relatively large considering the particle/crystallite sizes of the prepared materials, and thus the result may be considered fairly well representative. All the spectra are calibrated with respect to carbon position centered at 284.5 eV.

2.3. Catalytic tests

The batch catalytic experiments were performed in tubular glass reactors with pear-shaped bottoms and equipped with an appropriate PTFE-coated magnetic stirring bar and a valve. In a typical procedure, 0.45 M of furfural (Fur), powdered catalyst (loading of 26.7 g_{cat} dm^{-3}), and 0.75 mL of 2-butanol were added to the reactor, and heated at 120 °C. These reaction conditions are similar to those used by Bui et al. [63]. The choice of a secondary alcohol solvent was based upon the fact that they tend to be more efficient H-donors than primary alcohols for CTH reactions [67]. Catalytic tests were also carried out using furfuryl alcohol (FA), 1-butyl levulinate (1BL), α-angelica lactone (α-AnL), levulinic acid (LA), and ethyl furfuryl ether (EMF) as substrates. The reaction mixtures were heated with a thermostatically controlled oil bath, under continuous magnetic stirring at 1000 rpm. Zero time (the instant the reaction began) was taken to be the instant the reactor was immersed in the oil bath. Comparisons are based on the mass of catalyst (kept constant for all experiments), which is interesting from the point of view of practical application.

After a 7 h-batch run of Fur conversion (for Zr-TUD-1 and ((Zr)$_{SSIE}$-beta), the solid catalysts were separated from the reaction mixture by centrifugation, thoroughly washed with 2-butanol, and dried at 85 °C overnight (the obtained solids were brownish in colour, whereas the unused solids were white). The used catalysts were thermally treated under air at 550 °C for 3 h (heating rate of 1 °C min^{-1}) in order to remove carbonaceous matter. The regenerated catalysts were reused (total of seven batch runs) under similar reaction conditions.

In order to check for soluble active species, contact tests were carried out for the Zr-containing materials, as follows: the original catalyst was contacted with 2-butanol, at 120 °C, for 24 h, using similar conditions to those used for a typical catalytic run, but without substrate. Subsequently, the mixture was cooled to room temperature. The solid phase was separated by centrifugation, and dried at 85 °C, under atmospheric air. The dried solid (white coloured powder) was used for a batch run of Fur conversion. On the other hand, the (liquid) supernatant of the centrifugation process was passed through a filter containing a 0.2 μm PTFE membrane, and the liquid was transferred to a separate reactor; the substrate was added to give an initial concentration of 0.45 M, and the reaction solution was stirred at 120 °C.

2.4. Quantification and identification of the reaction products

The evolution of the catalytic reaction was monitored by GC (for quantification of the bio-products) and HPLC (for quantification of Fur). Prior to sampling, the reactors were cooled to ambient temperature before opening and work-up procedures. The analyses were always carried out for freshly prepared samples. The GC analyses were carried out using a Varian 3800 equipped with a capillary column (Chrompack, CP-SIL 5CB,

50 m × 0.32 mm × 0.5 μm) and a flame ionisation detector, using H_2 as carrier gas. The HPLC analyses were carried out using a Knauer Smartline HPLC Pump 100 and a Shodex SH1011H$^+$ 300 mm × 8 mm (i.d.) ion exchange column (Showa Denko America, Inc., New York), coupled to a Knauer Smartline UV detector 2520 (254 nm); the mobile phase was 0.005 M aq. H_2SO_4 at a flow rate of 0.8 mL min^{-1}, and the column temperature was 50 °C. Calibration curves were measured for quantification. Individual experiments were performed for a given reaction time and the presented results are the mean values of at least two replicates.

The substrate (sub) conversion (%) at reaction time t was calculated using the formula: 100 × [(initial concentration of sub)-(concentration of sub at time t)]/(initial concentration of sub). The yield of product (pro) (%) at reaction time t was calculated using the formula: 100 × [(concentration of pro at time t)/(initial concentration of sub)]. The bio-products (whenever formed) were furfuryl alcohol (FA), 2-butyl furfuryl ether (2BMF), levulinate ester (2BL = 2-butyl levulinate), angelica lactones (α-AnL = α-angelic lactone, β-AnL = β-angelic lactone), levulinic acid (LA), and γ-valerolactone (GVL).

The reaction products of the one-pot conversion of Fur in the presence of $(Zr)_{SSIE}$-beta, at 24 h and 120 °C were analysed by SPME/GC × GC-ToFMS. The injection port (250 °C) was lined with a 0.75 mm I.D. splitless glass liner and splitless injections were used (30 s). The LECO Pegasus 4D (LECO, St. Joseph, MI, USA) GC × GC-ToFMS system consisted of an Agilent GC 7890A gas chromatograph, with a dual stage jet cryogenic modulator (licensed from Zoex) and a secondary oven. The detector was a high-speed ToF mass spectrometer. A non-polar/polar set of columns was used: an equity-5 column (30 m × 0.32 mm I.D., 0.25 μm film thickness, J&W Scientific Inc., Folsom, CA, USA) was used as the first-dimension column and a DB-FFAP (1.00 m × 0.25 mm I.D., 0.25 μm film thickness, J&W Scientific Inc., Folsom, CA, USA) was used as the second-dimension column. The carrier gas was He at a constant flow rate of 2.0 mL min^{-1}. The primary oven temperature started at 35 °C during 0.2 min and then was programmed from 35 °C to 50 °C at a heating rate of 2 °C min^{-1}, then to 220 °C (14 min) at a heating rate of 5 °C min^{-1}; the secondary oven temperature started at 50 °C for 0.2 min, then from 50 °C to 65 °C at a heating rate of 2 °C min^{-1}, and then to 235 °C (14 min) at a heating rate of 5 °C min^{-1}. The temperature of the MS transfer line and the MS source was 250 °C. The modulation time was 5 s, and the modulator temperature was kept at 20 °C offset (above primary oven). The ToFMS was operated at a spectrum storage rate of 100 spectra s^{-1}. The mass spectrometer was operated in the EI mode at 70 eV using a range of m/z 30–500 and the detector voltage was ca. −1439 V. Total ion chromatograms (TIC) were processed using the automated data processing software ChromaTOF (LECO) at a signal-to-noise threshold of 100. Two commercial databases (Wiley 275 and US National Institute of Science and Technology (NIST) V. 2.0—Mainlib and Replib) were used. The majority of the identified compounds showed mass spectral similarity matches >840/1000. Furthermore, a manual inspection of the mass spectra was done, combined with the use of additional data, such as the retention index (RI) value, which was determined according to the van den Dool and Kovats RI equation [84]. For the determination of RI, a C8–C20 n-alkane was used, and as some volatile compounds were eluted before C8, the solvent n-hexane was used as C6 standard. The experimentally calculated RI values were compared, when available, with values reported in the literature for similar chromatographic columns employed in the first dimension.

On a routine basis, the identification of the bio-products was checked by GC–MS using a Trace GC 2000 Series (Thermo Quest CE Instruments)—DSQ II (Thermo Scientific), equipped with a capillary column (DB-5 MS, 30 m × 0.25 mm × 0.25 μm), using He as carrier gas.

2.5. Kinetic modelling

The micro reactors were modelled as perfectly stirred batch reactors, similar to that described previously by our group [46]. The mass balance equations are given by:

$$\frac{V}{W}\frac{dC_i}{dt} = r_i \qquad\qquad \text{Eq. (1)}$$

where V is the reaction mixture volume (L), W is the mass of catalyst (g), C_i is the molar concentration of the reactive species i (M), t is time (h), and r_i is the overall reaction rate of species i expressed per unit of mass of catalyst (mol g_{cat}^{-1} h^{-1}). The ratio W/V was maintained constant in all experiments.

Based on the mechanism proposed discussed in Section 3.2.3 (and represented in Fig. 9), a pseudo-homogeneous kinetic model was developed, considering first-order reactions for all steps involved. Possible loss-reactions of the species involved were considered, since, in general, the mole balances did not close for different bio-products as substrates (D_m denotes by-products formed from species m, and m is Fur, FA, 2BMF, AnLs, LA, 2BL or GVL).

$$\frac{V}{W}\frac{dC_{FUR}}{dt} = -\left(k_1 + k_9\right)C_{FUR} \qquad\qquad \text{Eq. (2)}$$

$$\frac{V}{W}\frac{dC_{FA}}{dt} = k_1\,C_{FUR} - \left(k_2 + k_3 + k_{10}\right)C_{FA} \qquad\qquad \text{Eq. (3)}$$

$$\frac{V}{W}\frac{dC_{2BMF}}{dt} = k_2\,C_{FA} - \left(k_4 + k_5 + k_{11}\right)C_{2BMF} \qquad\qquad \text{Eq. (4)}$$

$$\frac{V}{W}\frac{dC_{AnLs}}{dt} = k_3\,C_{FA} + k_4\,C_{2BMF} - \left(k_6 + k_{12}\right)C_{AnLs} \qquad\qquad \text{Eq. (5)}$$

$$\frac{V}{W}\frac{dC_{LA}}{dt} = k_6\,C_{AnLs} - \left(k_7 + k_{13}\right)C_{LA} \qquad\qquad \text{Eq. (6)}$$

$$\frac{V}{W}\frac{dC_{2BL}}{dt} = k_5\,C_{2BMF} + k_7\,C_{LA} - \left(k_8 + k_{14}\right)C_{2BL} \qquad\qquad \text{Eq. (7)}$$

$$\frac{V}{W}\frac{dC_{GVL}}{dt} = k_8\,C_{2BL} \qquad\qquad \text{Eq. (8)}$$

$$\frac{V}{W}\frac{dC_{\mathrm{D_{Fur}}}}{dt} = k_9\,C_{\mathrm{Fur}} \qquad\qquad\qquad \text{Eq. (9)}$$

$$\frac{V}{W}\frac{dC_{\mathrm{D_{FA}}}}{dt} = k_{10}\,C_{\mathrm{FA}} \qquad\qquad\qquad \text{Eq. (10)}$$

$$\frac{V}{W}\frac{dC_{\mathrm{D_{2BMF}}}}{dt} = k_{11}\,C_{\mathrm{2BMF}} \qquad\qquad\qquad \text{Eq. (11)}$$

$$\frac{V}{W}\frac{dC_{\mathrm{D_{AnLs}}}}{dt} = k_{12}\,C_{\mathrm{AnLs}} \qquad\qquad\qquad \text{Eq. (12)}$$

$$\frac{V}{W}\frac{dC_{\mathrm{D_{LA}}}}{dt} = k_{13}\,C_{\mathrm{LA}} \qquad\qquad\qquad \text{Eq. (13)}$$

$$\frac{V}{W}\frac{dC_{\mathrm{D_{2BL}}}}{dt} = k_{14}\,C_{\mathrm{2BL}} \qquad\qquad\qquad \text{Eq. (14)}$$

where k_j are the apparent reaction kinetic constants (L g_{cat}^{-1} h^{-1}) of step j at constant temperature.

Fig. 1. (a) PXRD patterns of modified beta materials and bulk ZrO_2, and (b) low angle PXRD patterns of TUD-1 type materials; "used" refers to solids recovered after catalytic reaction of Fur.
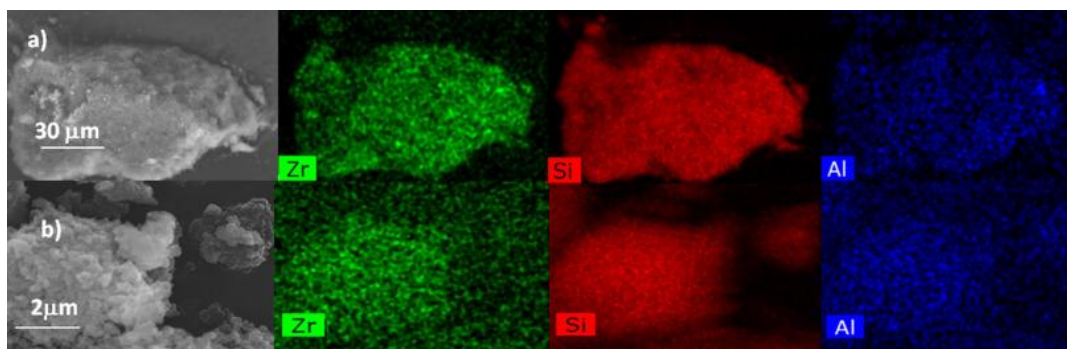
Fig. 2. SEM and mapping of Al, Si and Zr for (a) $(Zr)_{SSIE}$-beta and (b) $(ZrAl)_{SSIE}$-beta.
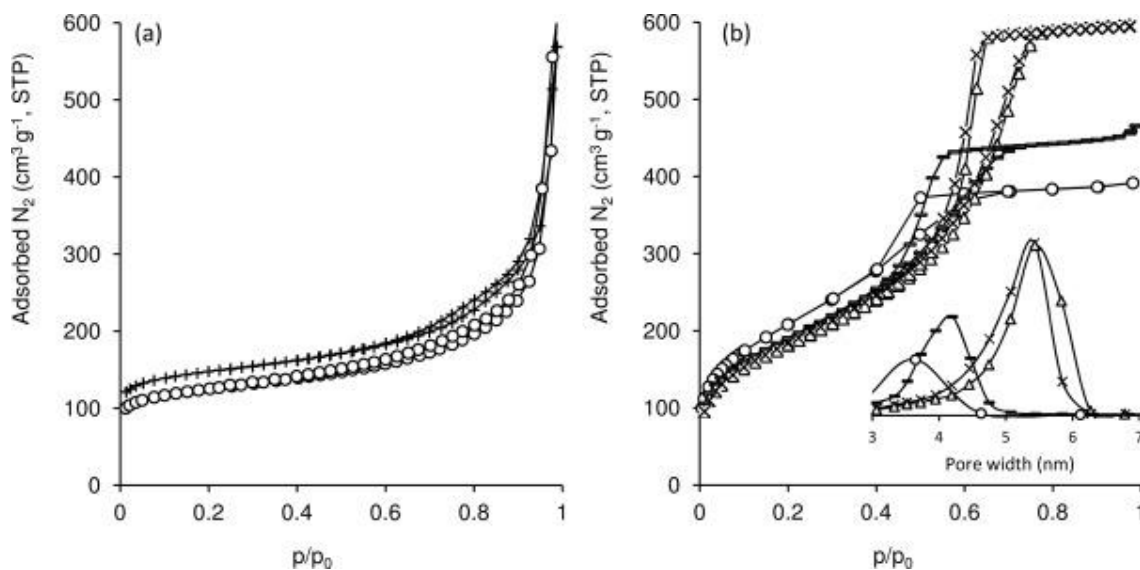
Fig. 3. Nitrogen adsorption–desorption isotherms at −196 °C for the (a) modified beta materials ($(Zr)_{SSIE}$-beta (o); $(ZrAl)_{SSIE}$-beta (+)), and (b) TUD-1 type materials where the inset shows the corresponding pore size distribution curves (Zr-TUD-1 (−), ZrAl-TUD-1(0.3) (Δ), ZrAl-TUD-1(0.7) (×), Al-TUD-1 (o)).
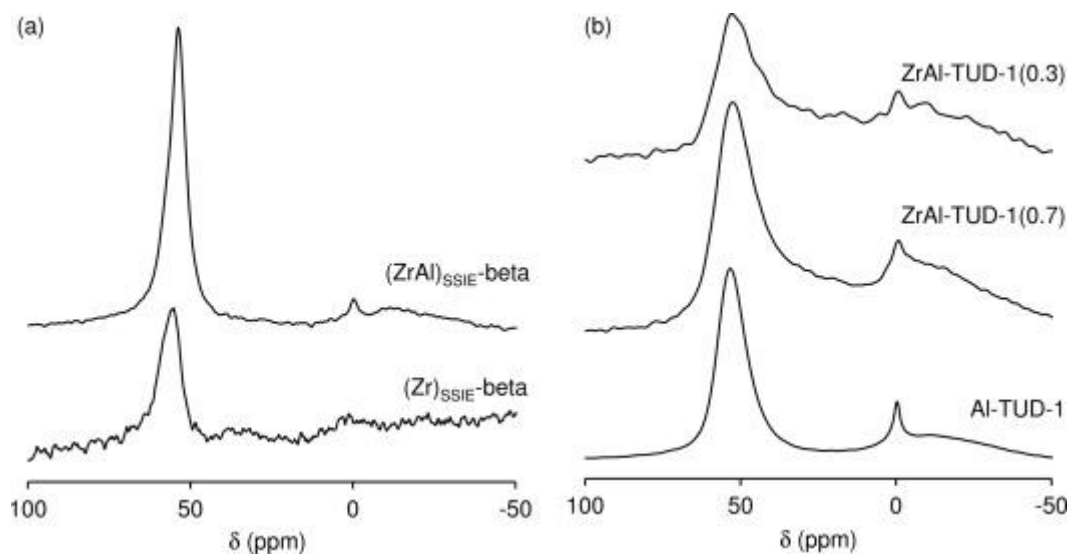
Fig. 4. ^{27}Al MAS NMR spectra of (a) beta and (b) TUD-1 type materials.
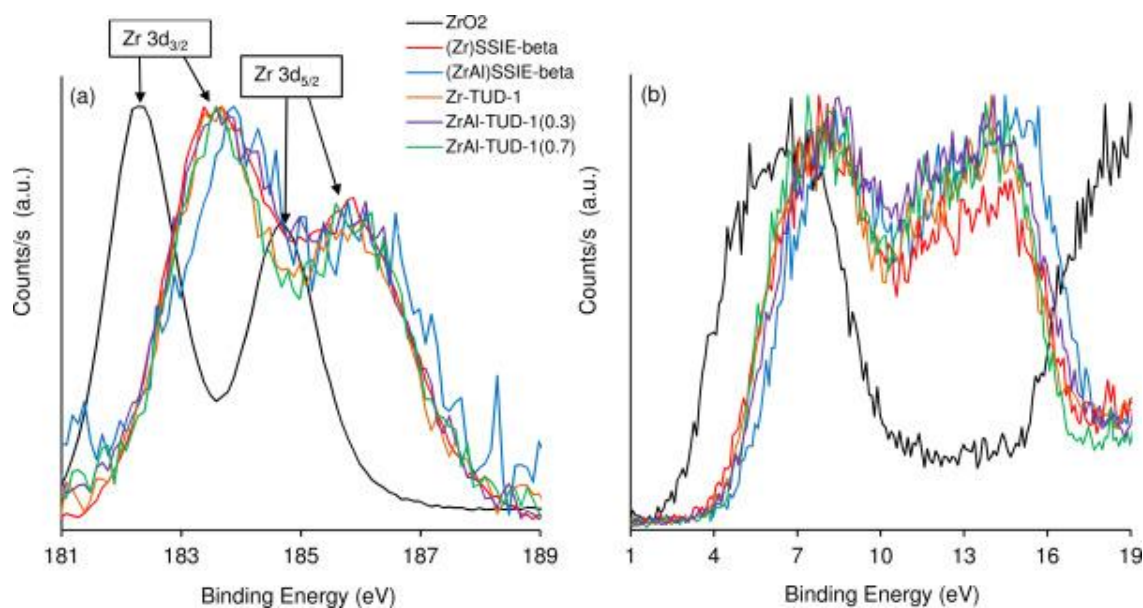
Fig. 5. Zr 3d core level (a) and valence band (b) spectra of beta and TUD-1 type materials.
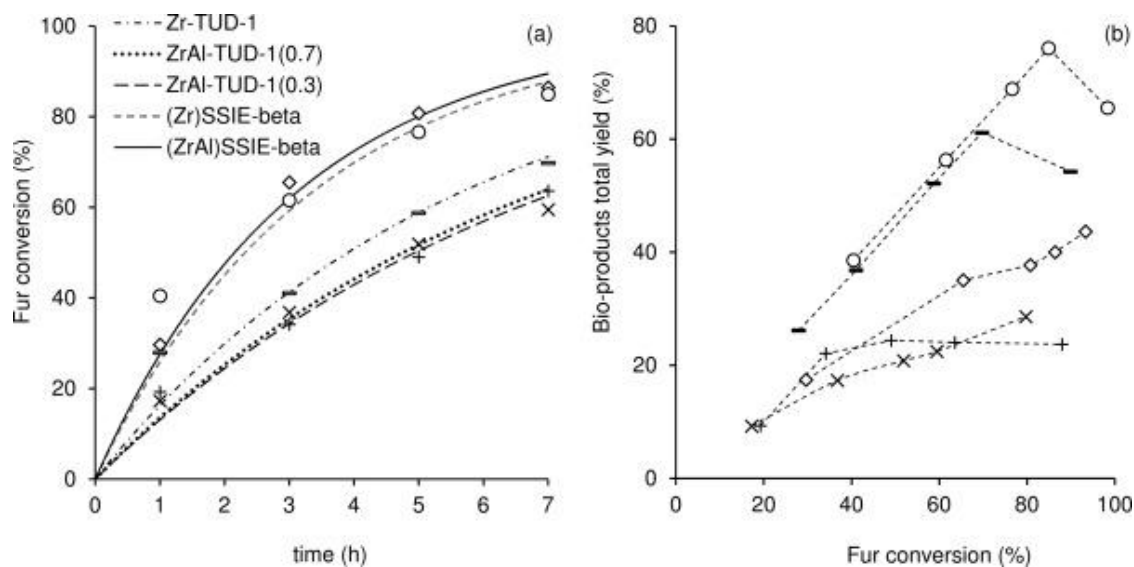
Fig. 6. Dependence of (a) Fur conversion on reaction time and (b) bio-products total yields on Fur conversion, in the presence of Zr-TUD-1 (−), ZrAl-TUD-1(0.3) (+), ZrAl-TUD-1(0.7) (×), (Zr)$_{SSIE}$-beta (o) or (ZrAl)$_{SSIE}$-beta (◊), in 2BuOH, at 120 °C. The lines in (a) are the curves calculated by kinetic modelling. The dashed lines in (b) are visual guides.

12
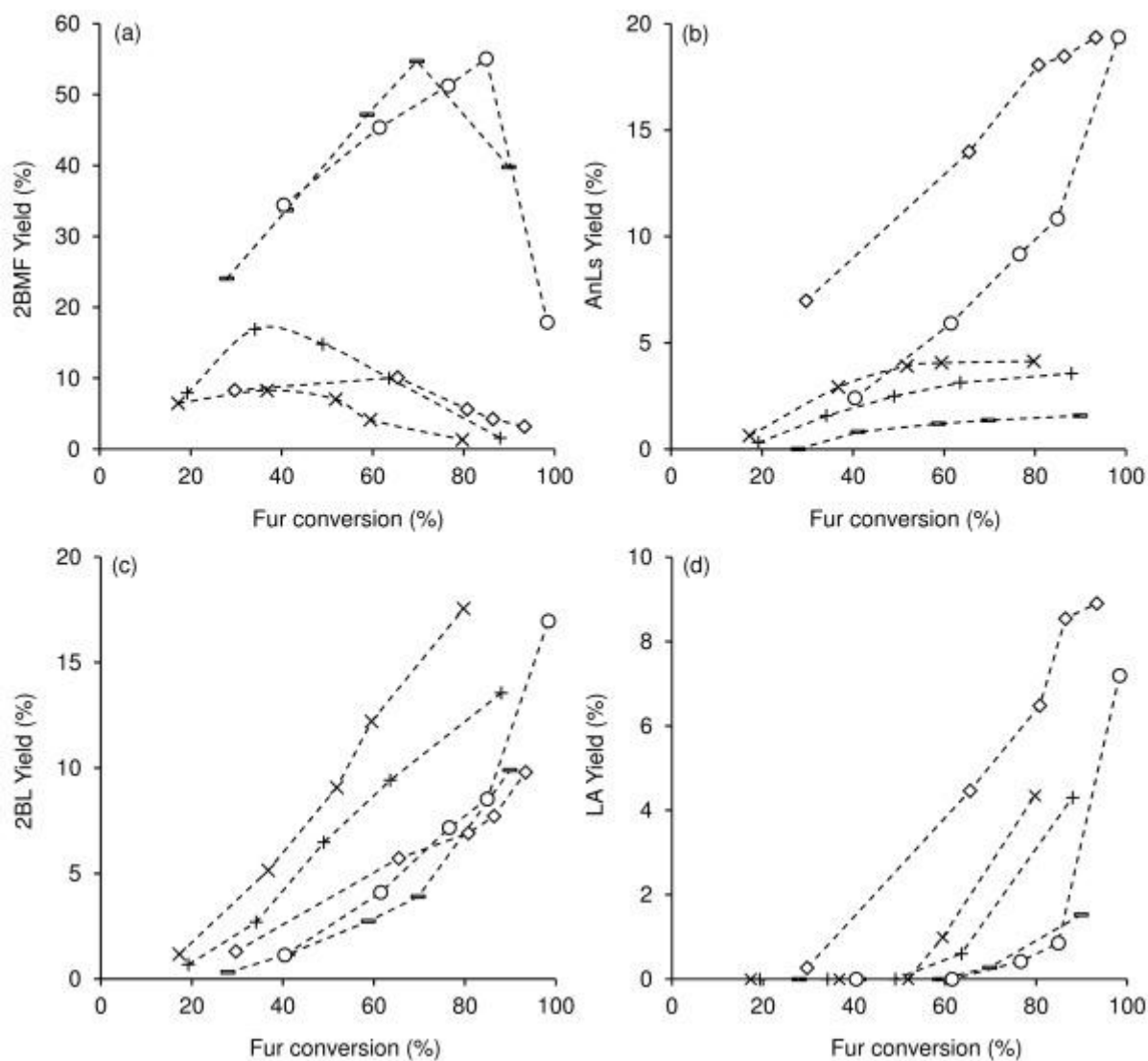
Fig. 7.

Dependence of the yields of 2BMF (a), AnLs (b), 2BL (c) and LA (d) on Fur conversion, in the presence of Zr-TUD-1 (−), ZrAl-TUD-1(0.3) (+), ZrAl-TUD-1(0.7) (×), (Zr)$_{SSIE}$-beta (o) or (ZrAl)$_{SSIE}$-beta (◊), in 2BuOH, at 120 °C. The dashed lines are visual guides.
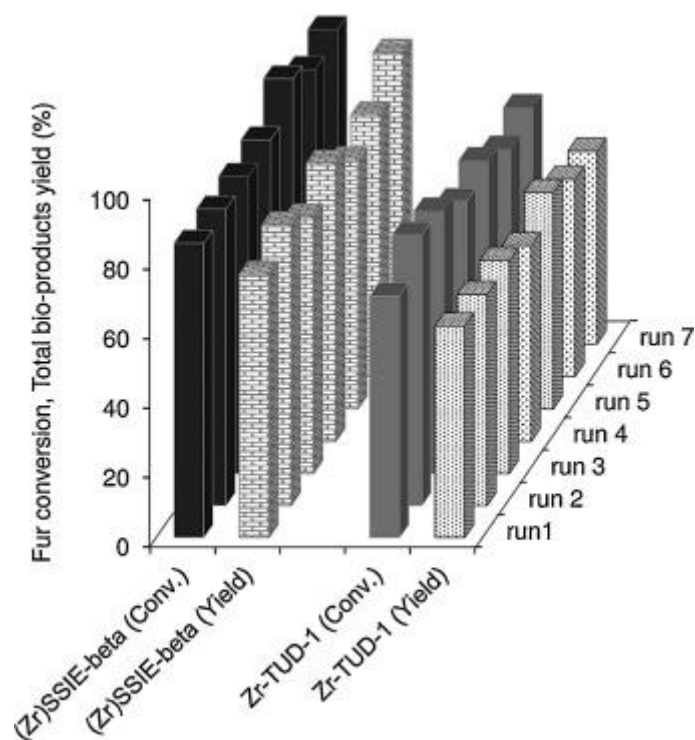
Fig. 8. Catalytic results for (Zr)$_{SSIE}$-beta and Zr-TUD-1 used for seven consecutive batch runs of Fur reaction with 2BuOH, at 120 °C.
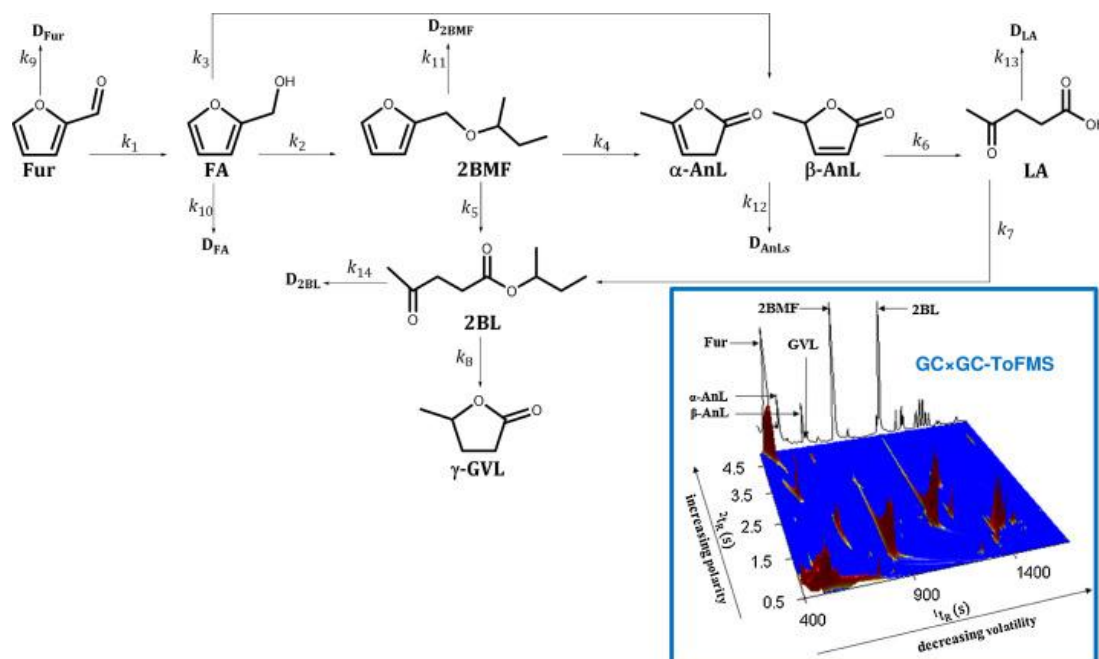
Fig. 9. Proposed overall reaction mechanism (top) of the integrated reduction-acid catalysed conversion of Fur in 2BuOH. TIC GC × GC-ToFMS contour plot representation (one- and three-dimensional) of the reaction mixture of Fur, in the presence of (Zr)$_{SSIE}$-beta (24 h, 120 °C) (right 3D plot).

The problem was solved by numerical integration with simultaneous optimisation, using appropriate initial conditions (at t = 0). MEIGO (Metaheuristics for systems biology and bIoinformatics Global Optimization) [85] an open-source toolbox for global optimisation, and Matlab® (version 7.8) were used to obtain the kinetic constants by

14

fitting the model proposed to the experimental data (up to 7 h) in order to minimise the following objective function:

$$F_{\mathrm{obj}} = \sum_{m} \left\{ \sum_{n=1}^{n_{\mathrm{p}}} \left[C_{m,n}\big|_{\mathrm{calc}} - C_{m,n}\big|_{\mathrm{exp}} \right]^2 \right\}$$

Eq. (15)

where $C_{m,n}|_{\mathrm{calc}}$Cm,n|calc and $C_{m,n}|_{\mathrm{exp}}$Cm,n|exp are the concentrations predicted by the model and the experimental ones, respectively, at each instant of time n.

3. Results and discussion

3.1. Characterisation of the catalysts

3.1.1. Beta type materials

In order to introduce tetrahedral Zr-sites into the BEA framework H-beta was partially dealuminated (deAl) to create vacant tetrahedral sites (giving deAl-beta), which were subsequently occupied by zirconium species introduced by solid-state ion-exchange (SSIE) giving $(Zr)_{SSIE}$-beta, or by zirconium and aluminium species giving $(ZrAl)_{SSIE}$-beta (Table 1). The Zr-free materials H-beta and deAl-beta were previously characterised by our group, and the results are reported in Ref. [46].

Table 1. Amounts of Zr and/or Al used in the preparation of the modified beta and

TUD-1 type materials, and textural properties.

Sample	Amounts of Zr, Al used for preparation	Textural properties	
		S_{BET} (m^2g^{-1})	V_p (cm^3g^{-1})
$(ZrAl)_{SSIE}$-beta	0.422(Zr)+0.422(Al) mmol/g$_{deAl-beta}$ (SSIE) [a]	554 (173)[c]	0.67 (0.15)[d]
$(Zr)_{SSIE}$-beta	0.844(Zr) mmol/g$_{deAl-beta}$ (SSIE) [a]	465 (170)[c]	0.67 (0.12)[d]
Al-TUD-1	Si/Al = 25 (synth. gel) [b]	738	0.58
ZrAl-TUD-1(0.7)	Si/(Zr+Al)=21; Al/Zr=0.7 (synth. gel) [b]	672	0.92
ZrAl-TUD-1(0.3)	Si/(Zr+Al)=21; Al/Zr=0.3 (synth. gel) [b]	656	0.92
Zr-TUD-1	Si/Zr = 18 (synth. gel) [b]	693	0.71

The powder X-ray diffraction (PXRD) patterns of $(Zr)_{SSIE}$-beta and $(ZrAl)_{SSIE}$-beta show reflections which are characteristic of a BEA topology (Fig. 1a), similar to that reported in the literature for Zr-containing beta type materials synthesised via different methodologies [63], [70], [86], [87], [88], [89] and [90]. On the other hand, the PXRD patterns for $(Zr)_{SSIE}$-beta and $(ZrAl)_{SSIE}$-beta are similar to those reported for deAl-beta and H-beta, indicating that the crystalline structure was preserved during the modification treatments [46]. Bulk ZrO_2 exhibited characteristic reflections of the crystalline monoclinic phase (ICDD PDF4 + 2013 reference code no. 04-001-7279), with the most intense reflections at $2\theta = 28.13°$ and $31.57°$ (Fig. 1a) [91]. There was no evidence of crystalline zirconia in the patterns of the Zr-containing beta type materials, suggesting that Zr was homogeneously dispersed during the SSIE/calcination steps.

The SEM images of $(Zr)_{SSIE}$-beta and $(ZrAl)_{SSIE}$-beta showed aggregates of small pseudo-spherical shaped crystallites (Fig. 2), similar to that reported for the synthetic precursor materials H-beta and deAl-beta [46]. The elemental mappings showed fairly homogeneous metal dispersions; no particles of bulk zirconia or alumina were observed, which is consistent with the PXRD studies. The EDS analyses of $(Zr)_{SSIE}$-beta and $(ZrAl)_{SSIE}$-beta indicated that they possess similar atomic ratio Si/(Zr + Al) (16–19) (Table 2), which is consistent with the fact that the molar amounts of Zr or (Zr + Al) added to deAl-beta were the same for the two materials (Table 1). The atomic ratio Al/Zr was higher for $(ZrAl)_{SSIE}$-beta than $(Zr)_{SSIE}$-beta (1.2 and 0.03, respectively), and the Si/Al ratio was much lower for $(ZrAl)_{SSIE}$-beta (35 compared to 588 $(Zr)_{SSIE}$-beta), which is consistent with the fact that $(ZrAl)_{SSIE}$-beta was obtained via SSIE for both Zr and Al. ICP-AES analyses of $(Zr)_{SSIE}$-beta and $(ZrAl)_{SSIE}$-beta gave roughly comparable results to the EDS analyses. Hence, metal dispersions may be considered fairly homogeneous for the two materials.

Table 2. Compositions of beta and TUD-1 type silicates before and after catalytic reaction of Fur.

Sample^a	Molar ratios (ICP-AES)				Molar ratios (EDS)			
	Si/Al	Si/Zr	Al/Zr	Si/(Zr+Al)	Si/Al	Si/Zr	Al/Zr	Si/(Zr+Al)
$(Zr)_{SSIE}$-beta	588	17	0.03	16	501	19	0.04	18
$(Zr)_{SSIE}$-beta used	582	17	0.03	17	513	21	0.04	20
$(ZrAl)_{SSIE}$-beta	35	40	1.2	19	37	34	0.9	18

(ZrAl)$_{SSIE}$-beta used	36	41	1.1	19	35	37	1.1	18
Zr-TUD-1	-	28	-	-	-	23	-	-
Zr-TUD-1 used	-	28	-	-	-	24	-	-
Zr-Al-TUD-1(0.3)	75	26	0.3	19	47	25	0.5	16
Zr-Al-TUD-1(0.7)	39	39	1	20	26	33	1.3	15
Zr-Al-TUD-1(0.7) used	39	39	1	20	28	30	1.1	15
Al-TUD-1	19	-	-	-	19	-	-	-

[b] "used" refers to solids recovered (washed and calcined) after catalytic reaction of Fur, at 120 °C.

The Zr-containing beta type materials exhibited N_2 adsorption isotherms of type I, featuring considerable N_2 uptake at low relative pressures ($p/p_0 < 0.1$) due to micropore filling, accounting for V_{micro} of ca. 0.14 cm^3 g^{-1} (Fig. 3a, Table 1). As p/p_0 approached unity, N_2 uptake was enhanced due to multilayer adsorption on the external surface of the crystallites, accounting for S_{ext} of ca. 172 m^2 g^{-1}, with S_{BET} in the range of 465–554 m^2 g^{-1}. The S_{ext} is similar to that reported for the parent zeolite H-beta (176 m^2 g^{-1}), which consists of nano-sized crystallites [92]. Hence, the textural properties were not considerably affected by the SSIE processes. The S_{BET} results are comparable to literature data for Al and/or Zr-containing beta type materials prepared via different synthetic methodologies [70], [86], [87], [88], [92], [93], [94], [95] and [96].

The ^{27}Al MAS NMR spectra of (Zr)$_{SSIE}$-beta and (ZrAl)$_{SSIE}$-beta showed a main peak at ca. 52 ppm, characteristic of (framework) Al-sites in tetrahedral coordination (Fig. 4a). The spectrum of (Zr)$_{SSIE}$-beta was similar to that reported for deAl-beta [46], suggesting that SSIE did not affect significantly the framework Al-sites of deAl-beta. The material (ZrAl)$_{SSIE}$-beta exhibited a much stronger resonance associated with tetrahedral Al-sites than (Zr)$_{SSIE}$-beta. Hence, the competitive SSIE for Zr + Al led to considerable reconstruction of framework tetrahedral Al-sites. Literature data for (Zr,Al)-containing beta materials obtained via seeded synthesis using HF as mineralizer, indicated the coexistence of tetra- and octahedral Al-sites [87]. The spectrum of (ZrAl)$_{SSIE}$-beta shows a very weak resonance at ca. 0 ppm due to Al-sites in octahedral coordination, which may be connected to the framework [97].

Fig. S1a compares the DR-UV spectra of the Zr-containing beta materials and bulk ZrO_2. Bulk ZrO_2 exhibits a prominent band at ca. 240 nm, which was not observed in the spectra of (Zr)$_{SSIE}$-beta and (ZrAl)$_{SSIE}$-beta. These results suggest that SSIE processes did not lead to formation of zirconium oxide particles, consistent with PXRD, SEM and elemental analyses.

The FT-IR spectra of (Zr)$_{SSIE}$-beta and (ZrAl)$_{SSIE}$-beta showed vibrational modes characteristic of the zeolite structure: 1218 cm^{-1}, 1086 cm^{-1}, 800 cm^{-1}, 580 cm^{-1},

520 cm^{-1} and 462 cm^{-1} (Fig. S2a) [98], [99], [100] and [101]. According to literature data for Zr- and (Zr,Al)-containing beta type materials, the band at ca. 1220 cm^{-1} may be assigned to asymmetric stretching vibrations of SiOT bridges (T = Al or Zr) [89]. Comparison of the spectra of (Zr)$_{SSIE}$-beta and (ZrAl)$_{SSIE}$-beta to that reported for deAl-beta [46], indicates that the relative intensity of the band at ca. 950 cm^{-1} decreased after SSIE. This band is assignable to SiO stretching vibrations of silanol groups present at connectivity defects [102] and [103]. Hence, decreased intensity of the absorbance at ca. 950 cm^{-1} suggests a lower amount of connectivity defects [102]. Accordingly, the SSIE process led to the insertion of Zr and/or Al at the defect sites of deAl-beta. This hypothesis is supported by the ^{27}Al MAS NMR results for (ZrAl)$_{SSIE}$-beta. The FT-IR spectrum of bulk ZrO_2 was different to those of (Zr)$_{SSIE}$-beta and (ZrAl)$_{SSIE}$-beta; no bands of bulk ZrO_2 could be differentiated in the spectra of the modified beta materials, which corroborates with fairly homogeneous metal dispersions in the modified materials.

The Zr-containing beta type materials and, for comparison, bulk ZrO_2, were characterised by X-ray photoelectron spectroscopy (XPS) in order to elucidate the type of Zr-sites in the materials. The Zr $3d_{5/2}$ and $3d_{3/2}$ spin-orbit doublet core level spectra of (Zr)$_{SSIE}$-beta and (ZrAl)$_{SSIE}$-beta were located at ca. 183.6 eV and 185.9 eV (Fig. 5a). These positions were well distinctly shifted with respect to those of bulk ZrO_2 located at 182.3 and 184.6 eV, and are assigned to framework Zr-sites [96] and [104]. The Zr 3d core level profiles of the zeotype materials were fairly well fitted considering the sole contribution of framework zirconium species (i.e. negligible contribution of ZrO_2). The valence band spectra shown in Fig. 5b confirmed further the differences between the beta type materials and bulk ZrO_2, indicating that (Zr)$_{SSIE}$-beta and (ZrAl)$_{SSIE}$-beta samples are essentially composed of framework Zr-sites.

The O1s core level profiles of the modified beta materials and bulk ZrO_2 were considerably different, consistent with the different chemical natures of the two types of materials (Fig. S3). Bulk ZrO_2 exhibited a band at ca. 530.4 eV, whereas the zeotype materials exhibited a band in the range 531.9–532.9 eV which is assignable to silicon–oxygen bonds [105], [106], [107], [108], [109], [110], [111], [112], [113], [114], [115] and [116]. The Si 2p core level spectra of (Zr)$_{SSIE}$-beta and (ZrAl)$_{SSIE}$-beta were roughly coincident, showing a band centered at ca. 104 eV (Fig. S4) [117]. The Al 2p core level spectrum of (ZrAl)$_{SSIE}$-beta showed a (poorly resolved) band at ca. 76 eV, which is in agreement with literature data for Al-containing beta type materials [117]; no band could be distinguished in the spectrum of (Zr)$_{SSIE}$-beta, likely due to sensitivity limits at low Al concentration (Fig. S4).

3.1.2. TUD-1 type materials

TUD-1 type materials were prepared by sol–gel/hydrothermal synthesis using different Al/Zr ratios, namely Al-TUD-1 (without Zr), Zr-TUD-1 (without Al) and (ZrAl)-TUD-1(x) (with Al and Zr, where x is the molar ratio Al/Zr of the corresponding synthesis gel).

The PXRD patterns of the TUD-1 type materials were similar, displaying a broad peak at low angle (centred at ca. 1–1.1° 2θ, Fig. 1b), and, on the other hand, a very broad peak at high angle (centred at ca. 24° 2θ, Fig. S5). These results are in agreement with literature data for similar materials possessing Al and/or Zr [82], [83], [118],

[119] and [120], and are consistent with the TUD-1 mesoporous structure formed by amorphous pore walls. There was no evidence of crystalline zirconia, suggesting fairly homogeneous metal dispersions.

The SEM images of the TUD-1 type materials showed particles of irregular shapes and sizes (Fig. S6), similar to that reported in the literature for TUD-1 type materials [81], [121] and [122]. The chemical mappings showed fairly homogeneous metal dispersions, and no particles of zirconia or alumina were observed, consistent with the respective PXRD data. The EDS analyses indicated atomic ratios of Si/Al = 19 for Al-TUD-1, and Si/Zr = 23 for Zr-TUD-1; these values are roughly comparable to the respective ratios of the corresponding synthesis gels (Table 1). The materials (ZrAl)-TUD-1(0.3) and (ZrAl)-TUD-1(0.7) possessed a similar Si/(Zr + Al) atomic ratio (15–16), and the atomic ratio Al/Zr which was 0.5 for (ZrAl)-TUD-1(0.3) and 1.3 for (ZrAl)-TUD-1(0.7). The compositions of the materials (Table 2) and the corresponding synthesis gels (Table 1) were somewhat comparable, suggesting fairly good synthesis method predictability of these types of mesoporous silicates, as previously reported by Hanefeld and colleagues [82], [83] and [118]. ICP-AES analyses of the TUD-1 type materials gave comparable results to the EDS analyses. Hence, metal dispersions may be considered fairly homogeneous for the two materials.

The materials prepared exhibited type IV adsorption isotherms, and a H-2 hysteresis loop in the relative pressure range (p/p_0) of ca. 0.4–0.75 (Fig. 3b). These features are consistent with the materials possessing mesoporosity and an interconnected pore network, where condensation and evaporation may occur via different mechanisms [123], [124] and [125]. The N_2 uptake reached a plateau at high p/p_0, indicating negligible secondary mesopores or macropores, which is in agreement with the literature for purely siliceous, as well as Al and/or Zr-containing TUD-1 type materials [75], [82], [118], [126], [127], [128] and [129]. Based on the mesopore size distribution curves (Fig. 3b inset), the Zr-containing materials seem to possess larger pore sizes than Al-TUD-1; 5.4 nm for (ZrAl)-TUD-1(0.3) and (ZrAl)-TUD-1(0.7), 4.2 nm and 3.6 nm for Zr-TUD-1 and Al-TUD-1, respectively. These results may be partly due to the introduction of relatively bulky zirconium atoms into the framework [118], and/or to differences in rates of hydrolysis and condensation reactions of the metal precursors during sol-gel synthesis [128].

The ^{27}Al MAS NMR spectra of the Al-containing TUD-1 type materials are similar, showing a strong resonance at ca. 50 ppm assigned to tetrahedral Al-sites, and a weaker signal at ca. 0 ppm due to hexacoordinated Al-sites (Fig. 4b). For the three materials, the peak at ca. 50 ppm is relatively broad, and seems to possess a shoulder at ca. 30 ppm, which may be due to pentacoordinated Al-sites. Similar spectral features have been reported in the literature for Al- [75], [127] and [130] and (Zr,Al)-containing [83] TUD-1 type materials.

The DR-UV spectra of the Zr-containing TUD-1 materials show a broad, weak band between 230 and 280 nm (Fig. S1b), which may be partly due to O^{2-} to Zr^{4+} charge transfer interactions with zirconium in low coordination states [82] and [118]. Bulk ZrO_2 exhibited a band at ca. 240 nm characteristic of zirconia materials [82], which was not observed for the Zr-containing TUD-1 materials prepared.

The FT-IR spectra of the TUD-1 type materials (Fig. S2b) show a typical band at ca. 1080 cm^{-1} and a shoulder at ca. 1200–1210 cm^{-1} assignable to asymmetric stretching vibrations of Si—O—Si bridges, and a band at ca. 795–810 cm^{-1} due to symmetric stretching vibration of Si—O—Si [83] and [118]. A band at ca. 960 cm^{-1} may be due to stretching vibrations of terminal silanol groups present at defect sites [131] and/or Si—O—Zr stretching vibrations (in Zr-containing materials) [118]. Similar spectral features have been reported in the literature for different types of Zr-containing ordered mesoporous silicates, such as Zr-MCM-41 [132] and [133] and Zr-MSU [134]. The spectrum of bulk ZrO$_2$ was different from those of the mesoporous silicates prepared; no bands of ZrO$_2$ could be distinguished in the spectra of the Zr-containing TUD-1 materials.

The Zr-containing TUD-1 materials were characterised by XPS in order to elucidate the type of Zr-sites. The Zr 3d$_{5/2}$ and 3d$_{3/2}$ spin-orbit doublet core level spectra of the mesoporous silicates were located at ca. 183.6 eV and 186 eV (Fig. 5a), which were distinct from those of bulk ZrO$_2$, and are assignable to framework Zr-sites [82], [83], [118] and [119]. The spectral contribution due to ZrO$_2$ bonds was negligible. The Zr 3d core level profiles of the mesoporous silicates were fairly well fitted considering only framework zirconium species. The valence band spectra of the TUD-1 type materials were considerably different from bulk ZrO$_2$ (Fig. 5b), confirming the differences between the two types of materials. The mesoporous silicates prepared are essentially composed of framework Zr-sites, similar to that observed for the zeotype materials prepared.
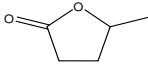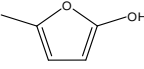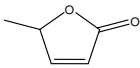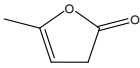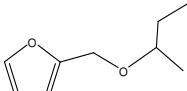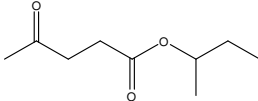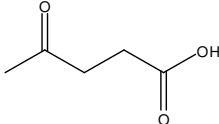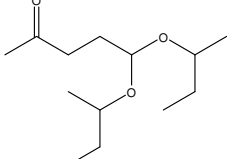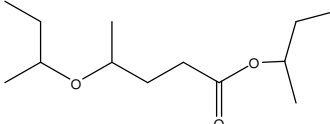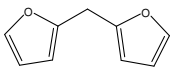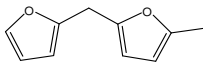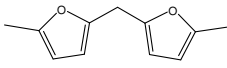
The TUD-1 type materials exhibited an O1s core level band centred at ca. 533 eV, assignable to silicon–oxygen bonds (Fig. S3) [82], [83], [118] and [119]. The O 1s core level spectra of these materials resembled somewhat closely those of the beta type materials prepared, and, on the other hand, were significantly different from that of bulk ZrO$_2$. These results may be partly related to the fact that the metallosilicates consist essentially of oxygen atoms bonded to T atoms (T = Si, Al and Zr) in tetrahedral coordination, whereas bulk ZrO$_2$ is essentially of polymeric nature possessing Zr—O—Zr moieties. The Si 2p core level spectra of the TUD-1 type materials were roughly coincident, showing a band centered at ca. 103.5 eV (Fig. S4). The Al 2p core level spectra of the materials (ZrAl)-TUD-1(x) showed a (poorly resolved) band at ca. 76 eV in agreement with literature data for TUD-1 type aluminosilicates (Fig. S4) [83].
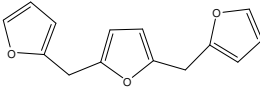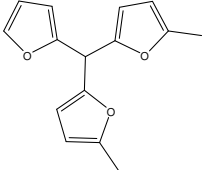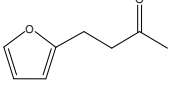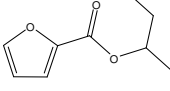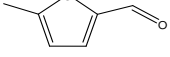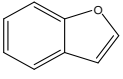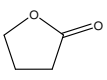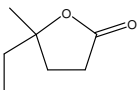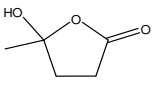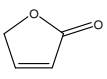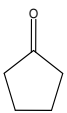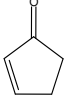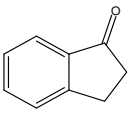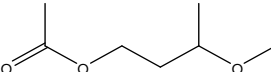
3.2. Catalytic tests
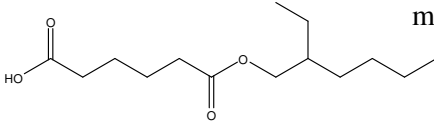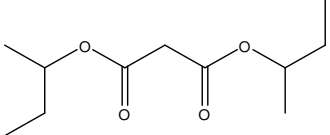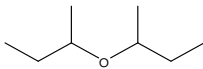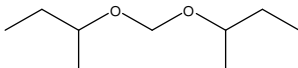
3.2.1. General considerations

The (Zr,Al)-containing zeolite beta and TUD-1 type materials prepared were investigated for the reaction of Fur to bio-products, in 2-butanol, at 120 °C. All Zr-containing silicates promoted the conversion of Fur (Fig. 6). The GC × GC-ToFMS analyses of the reaction mixture led to the identification of the bio-products 2BMF, 2BL, AnLs, FA and GVL, as well as by-products; exemplified for (Zr)$_{SSIE}$-beta in Table 3, indicating the experimentally calculated and, when available, published RI values [121], [135], [136], [137], [138], [139], [140], [141], [142] and [143]. The mass fragmentation patterns for some products are given in Section S.2 of the Supplementary data. LA was identified by GC–MS. The isomerisation of αAnL to βAnL occurred with time (the latter is more stable [144]).

Table 3. Products detected by GC×GC-ToFMS for the reaction of Fur with 2-BuOH, in the presence of (Zr)$_{SSIE}$-beta, at 120 ºC. [a]

Reaction Product		Sim. [b]	RI [c].	RI [Ref.] [d]
Molecular structure	Name of compound			
	γ-valerolactone [e]	966	975	978 [135]
	furfuryl alcohol	938	907	880 [136]
	β-angelica lactone	939	963	960 [121]
	α-angelica lactone	870	905	895 [121]
	2-butyl furfuryl ether	-	1051	-
	2-butyl levulinate [e]	-	1197	-
	levulinic acid [f]	-	-	-
	5,5-di-sec-butoxypentan-2-one	-	1615	-
	sec-butyl-4-sec-butoxypentanoate	-	1441	-
Furan-based by-products				
	2,2'-methylenebis(furan)	925	1091	1084 [121]
	2-(2-furanylmethyl)-5-methylfuran	936	1182	1179 [121]
	2,2'-methylenebis(5-methylfuran)	932	1277	1277 [121]

	2,5-bis(2-furanylmethyl)-furan	879	1654	1650 [121]
	2,2'-(2-furylmethylene)bis(5-methylfuran)	873	1631	1627 [121]
	1-(2-furyl)-butan-3-one	859	1084	1077 [121]
	sec-butyl-2-furoate [e]	-	1188	-
	5-methyl-furfural	967	986	980 [121]
	benzofuran	917	1008	1006 [137]

Others

	butyrolactone	915	942	938 [138]
	γ-Methyl-γ-ethylbutyrolactone [e]	890	1099	1095 [139]
	5-hydroxy-5-methyldihydrofuran-2(3H)-one [e] (Pseudo LA)	-	1096	-
	2(5H)-furanone	961	950	918 [140]
	cyclopentanone	914	817	808 [141]
	2-cyclopenten-1-one	949	880	890 [144]
	indanone	913	1278	1286 [143]
	1-butanol, 3-methoxy-, acetate [e]	961	998	-

Structure	Name	Similarity[b]	RI[c]	Lit. RI[d]
	mono(2-ethylhexyl)ester hexanedioic acid	900	2388	-
	di-sec-butyl malonate [e]	841	1330	-

Products from 2BuOH

Structure	Name	Similarity[b]	RI[c]	Lit. RI[d]
	di-sec-butyl ether	919	842	860 [121]
	di-(2-butoxy)methane	900	1000	-

[a] Reaction conditions: $[Fur]_0 = 0.45$ M in 2BuOH, 27 $g_{cat}L^{-1}$, 24 h, 120 °C. The listed products were generally formed for other Zr-containing catalysts. [b] Similarity (described in section 2.4). [c] Retention index (RI) obtained through the modulated chromatogram. [d] Retention index reported in the literature for one dimensional GC with 5%-phenyl-methylpolysiloxane GC column or equivalent. [e] Compound also identified with LA as substrate. [f] Identified by GC-MS.

Fig. 7 shows the bio-product yield versus Fur conversion and Fig. S10 of the Supplementary data presents the bio-product yield versus Fur reaction time. The highest total yield of bio-products was observed for $(Zr)_{SSIE}$-beta (76% yield at 85% Fur conversion) where 2BMF was predominant (55% yield, Fig. 7a). The catalytic performance of $(Zr)_{SSIE}$-beta is comparable to that reported recently for a related tin-containing material $(Sn)_{SSIE}$-beta, which was prepared from the same deAl-beta precursor tested under identical Fur reaction conditions [46], exhibiting 83% bio-products total yield at ca. 85% conversion, with 2BMF as predominant bio-product (58% yield). An advantage of $(Zr)_{SSIE}$-beta is that its composition is more eco-friendly than the related Sn-containing catalytic material.

The catalytic results of $(Zr)_{SSIE}$-beta may be compared with the innovative work by Bui et al. [63] for similar Fur reaction conditions, using a Zr-beta sample as sole catalyst (Al-free, and prepared via HF-based prolonged hydrothermal synthesis), or mechanically mixed with H$^+$-form zeolite beta (denoted herein as Zr-beta/Al-beta for the sake of simplicity). Results for $(Zr)_{SSIE}$-beta more closely resemble those reported for Zr-beta/Al-beta than for the Zr-beta catalyst [63]; the latter led to a mixture of FA and 2BMF in a total yield of 94%, whereas Zr-beta/Al-beta led to a bio-products spectrum (FA, 2BMF, 2BL, AnLs, LA and GVL) which was similar to that observed for $(Zr)_{SSIE}$-beta of the present work. The greater similarities between $(Zr)_{SSIE}$-beta and Zr-

beta/Al-beta may be due to the coexistence of Al- and Zr-sites for both one-pot reaction systems. However, while the total yields of bio-products were comparable for $(Zr)_{SSIE}$-beta and Zr-beta/Al-beta, the individual yields were different, especially of GVL (44% for Zr-beta/Al-beta [63], and only 4% for $(Zr)_{SSIE}$-beta at 24 h). The differences in the individual yields may be partly due to various physicochemical differences between $(Zr)_{SSIE}$-beta and Zr-beta/Al-beta (composition, textural and morphological properties).

For improved designs of eco-friendly ZrAl-containing ordered micro/mesoporous catalytic materials it is important to assess catalyst stability and understand the influence of material properties on the catalytic process. For these aims, systematic catalytic tests and characterisation studies were carried out for the Zr/Al-containing beta and TUD-1 type materials to check catalyst stability (Section 3.2.2), and to gain insights into mechanisms (Section 3.2.3) and roles of Zr- and Al-sites on each step of the overall Fur conversion (Section 3.2.4). For each family of materials a great care was taken to produce materials with comparable (and favourable) textural properties (Table 1) so that the observed differences in catalytic performances could be essentially attributed to the respective active sites (Section 3.2.4).

3.2.2. Catalyst stability

Excellent stability is an important requirement for the practical application of eco-friendly catalysts. The stability of the Zr-containing beta and TUD-1 type materials prepared was checked by carrying out contact tests (CT), under similar conditions to those used for the catalytic reaction of Fur, but without substrate (details in the Section 2). The solid (denoted as CT-S) and liquid phases (CT-L) obtained from the CTs were used separately for the reaction of Fur in heterogeneous and homogeneous phase, respectively. For all materials, the CT-L solutions led to negligible bio-products (<1.5% yield, Fig. S11), suggesting the absence of soluble active species and good catalyst stability towards metal leaching. On the other hand, the catalytic tests with the solids CT-S led to roughly comparable results to those obtained in standard tests (Fig. S11).

The originally white powdered catalysts turned brownish during the typical batch runs, likely due to adsorbed carbonaceous matter (reaction by-products). DSC analyses of the spent (24 h batch run) and fresh catalysts showed endothermic bands below 200 °C, assignable to physisorbed water (exemplified for four samples in Fig. S7). Above 300 °C, the used catalysts exhibited exothermic bands, which were not observed for the fresh catalysts. The exothermic process can be attributed to the decomposition of organic matter on the used catalysts. The GC × GC-ToFMS analyses of the Fur reaction mixtures indicated the presence of bi- and tricyclic furan compounds, which may result from the condensation reactions (Table 3). For example, 2,2′-methylenebis(furan), 2-(2-furanylmethyl)-5-methylfuran, 2,2′-methylenebis(5-methylfuran), 2,5-bis(2-furanylmethyl) furan, 2,2′-(2-furanylmethylene)bis(5-methylfuran) and heterocyclic compounds consisting of benzene and furan rings (e.g. benzofuran) were formed. Similar types of byproducts may also be formed from FA [121] and [142]. From these results, it is possible that relatively high molecular weight by-products were formed and deposited on the catalyst surface.

Table 4. Catalytic performance of the beta and TUD-1 type silicates, and ZrO_2 in the

reaction of Fur and selected bio-products as substrates, at 120 ºC.[a]

Sample	Substrate (time)	Conv.[b] (%)	Bio-products yield (%)						Total yield (%) [c]
			FA	2BMF	2BL	LA	AnLs	GVL	
(Zr)$_{SSIE}$-beta	Fur (24 h)	98	1	18	17	7	19	4	66
(ZrAl)$_{SSIE}$-beta	Fur (24 h)	93	1	3	10	9	19	1	44
deAl-beta [42]	Fur (24 h)	24	1	2	1	-	1	-	5
H-beta[42]	Fur (24 h)	43	1	-	3	2	4	-	10
Zr-TUD-1	Fur (24 h)	87	1	25	10	4	2	<1	42
ZrAl-TUD-1(0.3)	Fur (24 h)	88	-	2	14	4	4	1	24
ZrAl-TUD-1(0.7)	Fur(24 h)	80	1	1	18	4	4	<1	28
Al-TUD-1	Fur (24 h)	22	1	-	-	-	-	-	1
ZrO$_2$	Fur (24 h)	19	<1	1	<1	-	1	<1	2
None	Fur (24 h)	9	1	-	-	-	-	-	1
(Zr)$_{SSIE}$-beta	FA (1 h)	100	-	49	4	-	14	-	67
(ZrAl)$_{SSIE}$-beta	FA (1 h)	100	-	22	5	1	28	-	56
deAl-beta	FA (1 h)	40	-	23	-	-	-	-	23
H-beta	FA (1 h)	100		11	10	17	15	-	53
Zr-TUD-1	FA (1 h)	83	-	61	1	-	3	-	65
ZrAl-TUD-1(0.3)	FA (1 h)	98	-	50	8	2	4	-	64
ZrAl-TUD-1(0.7)	FA (1 h)	100	-	15	15	7	11	-	48
Al-TUD-1	FA (1 h)	100	-	3	18	8	13	-	42
ZrO$_2$	FA (24 h)	0	-	-	-	-	-	-	-

Based on the TGA analyses of the spent catalysts, the total mass loss in the temperature range 300–550 °C was 15.8 and 17.3 wt.% for (Zr)$_{SSIE}$-beta and (ZrAl)$_{SSIE}$-beta, respectively, and 10.7, 12.5 and 14.6 wt.% for Zr-TUD-1, ZrAl-TUD-1(0.3) and ZrAl-

TUD-1(0.7), respectively. For the fresh catalysts the mass losses were less than 2%. The Al-richer catalysts tended to possess greater amount of by-products, which is consistent with the fact that they led to lower total yields of bio-products. For Zr-TUD-1 and $(Zr)_{SSIE}$-beta the bio-products total yield dropped at high conversions (Fig. 6), which may be partly due catalyst deactivation by deposited organic matter.

The carbonaceous matter was removed from the spent catalysts by thermal treatment at 550 °C. The PXRD patterns (Figs. 1 and S5), SEM (Figs. S8 and S9) and FT-IR spectra (Fig. S2) of the recovered catalysts were comparable to the corresponding data for the fresh catalysts, suggesting that the structural and morphological features of the catalytic materials were preserved. Moreover, the compositions and metal dispersions (ICP-AES and EDS (Table 2), and chemical distribution maps (Figs. S8 and S9)) of the spent solids were similar to those of the corresponding fresh catalytic materials.

Seven consecutive batch runs were carried out for Zr-TUD-1 and $(Zr)_{SSIE}$-beta, and no considerable differences in the catalytic performances were observed (Fig. 8). These results are consistent with the CTs, indicating fairly good catalyst stabilities. The stability of $(Zr)_{SSIE}$-beta (prepared via SSIE) is comparable to that reported in the literature for a Zr-beta sample prepared via 20-day hydrothermal synthesis and tested as catalyst for LA conversion in alcohol medium (the catalyst was calcined prior to reuse) [70].

3.2.3. Overall reaction mechanism

The mechanistic proposal presented in Fig. 9 for the overall Fur reaction is based on experimental and literature data discussed below. Scheme 1 shows the possible balanced stoichiometric chemical equations for some key reactions. Based on the bio-products spectrum obtained for each substrate using the Zr,Al-containing beta type catalysts (Table 4), the following cascade of reactions is likely involved in the overall Fur conversion: Fur-FA-FE-AnLs-LA-2BL-GVL (k_1, k_2, k_4, k_6, k_7, k_8, Fig. 9). The same series of steps seems to occur for the Zr-containing TUD-1 type materials. All catalysts possessed higher activity for FA conversion (83–100% conversion at 1 h reaction) than for Fur conversion (17–47% conversion at 1 h). The high reactivity of FA explains the low FA concentrations observed for the Fur system (Table 4). The conversion of Fur to 2BMF likely involves a catalytic transfer hydrogenation (CTH) reaction between Fur and 2BuOH (H-donor) giving FA (k_1, Fig. 9), followed by the acid-catalysed etherification of FA to 2BMF (k_2) which is further converted to other bio-products.

The formation of 2BL took place ahead of LA, since initially the 2BL yields were higher than of LA, and relatively long induction periods were observed for LA formation (Fig. S10). These results suggest that 2BL is not solely formed from LA (k_7, Fig. 9) according to the series of steps indicated above, but may be formed via parallel pathways. According to the literature, the Fur to LEs conversion can involve the intermediate formation of FA [20] and [145] and FEs [146] and [147], and, on the other hand, FA is converted to LEs via FEs [51], [53], [54] and [55] (Scheme 1). Some of us have previously reported that materials of the type Al-TUD-1 and H-beta promoted the acid-catalysed series of steps FA-FEs-LEs [121] and [142]. It has also been reported that Fur can be converted to LEs via the intermediate formation of αAnL [63] and [148]. Besides FEs and AnLs, we identified 5,5-di-sec-butoxypentan-2-one (DBP) by GC × GC-ToFMS analyses for the Fur reaction mixture using the Zr-containing

catalysts (Table 3). The compound DBP is similar to the previously reported intermediates 5,5-diethoxy-2-pentanone and 5,5-dibutoxy-2-pentanone formed in the conversion of FA to LEs in ethanol or 1-butanol medium, respectively [53], [121] and [142]. Based on the literature survey, FA may be converted to 2BL with (k_2, k_4, k_6, k_7, Fig. 9) or without (k_2 and k_5) the intermediate formation of AnLs.

For the Fur/2BuOH system, water was formed, which may lead to different pathways. For example, water is formed in the condensation of FA with 2BuOH to give 2BMF (Scheme 1), and in auto-condensation of 2BuOH to ethers (Table 3). The formation of 2BL via AnLs involves the hydration of αAnL to LA (k_6). It has been previously reported that aluminosilicate acid catalysts may promote the conversion of FA [37] and [56] and AnLs [149] to LA in aqueous phase. Gürbüz et al. [37] reported that the aqueous phase reaction of FA in the presence of zeolite H-ZSM-5 gave 15% LA yield at 100% FA conversion after 1 h at 125 °C [37]. In a different study, the same group proposed various pathways for the aqueous phase conversion of FA to LA, one of which involved the intermediate formation of protonated αAnL [57]. Hence, it is possible that in the overall Fur system, FA is converted to LA via different routes with (k_2, Fig. 9) or without (k_3) the intermediate formation of FEs.

For all silicate catalysts, the end bio-product GVL was formed from Fur with very low to negligible yields (Table 4). GVL may be formed from LA [67], [70] and [150] or LEs [20], [66], [67] and [68] in alcohol media via CTH reaction, in the presence of zirconium-containing catalysts. In the present study, *sec*-butyl-4-*sec*-butoxypentanoate was identified (Table 3). This compound may be formed from 4-hydroxypentanoate (HPE) which is an intermediate in the reaction of LEs to GVL (k_8, Fig. 9); HPE was not detected possibly due to its high reactivity [68].

3.2.4. Influence of material properties

In order to understand the influence of material properties on the different steps of the reaction network, comparative systematic studies were carried out for Zr-free and Zr-containing catalysts with Fur and selected bio-products as substrates (Table 4).

The initial Fur reaction rates were higher for the beta type catalysts (4.9–6.8 mmol g_{cat}^{-1} h^{-1}) than the TUD-1 type ones (2.8–4.7 mmol g_{cat}^{-1} h^{-1}). (ZrAl)$_{SSIE}$-beta was more active than ZrAl-TUD-1(0.7) (Fig. 6) despite their similar compositions (Table 2). No clear correlation could be established between catalytic activity and the textural properties for the two families of materials; the (less active) TUD-1 type materials possessed higher S_{BET}, V_p and pore sizes than the beta type ones (Table 1). These results suggest that the textural parameters are not factors ruling the catalytic activity. This can be supported by analysing the materials' textural properties. The microporous zeotype catalysts (prepared from nano-size crystallites of H-beta) possess significant external surface area/micropore volume ratios (Table 1), enabling relatively short diffusional paths of the molecules. On the other hand, the TUD-1 type catalysts possess mesoporous structure (3–5 nm pore widths, Fig. 3b inset), facilitating access to the active sites (the molecular diameter of Fur is ca. 0.57 nm along the longest axis [151]). Hence, the textural/morphological characteristics of the two families of materials seem to be favourable for Fur conversion, and the observed differences in catalytic performances may be essentially due to differences in type and/or number of active sites.

The observed catalytic activity can be seen as the integrated contributions of all active sites with different intrinsic activities. It has been reported that the overall activity of Zr-beta type materials may result from different contributions of framework sites at different crystallographic positions [152]. On the other hand, the structural order of the catalytic materials may affect the ranges of bond angles/lengths and ligand lability of the metal sites, with effects on intrinsic activity [153] and [154]. Accordingly, it may not be straightforward to establish relationships between the catalytic activity and active sites between different families of materials, such as zeolite beta and TUD-1 type materials. Although beta and TUD-1 type materials possess 3-D pore structures, they are crystallographically very different; the former with a BEA topology and crystalline walls (atom-level order) and the latter with a sponge/worm-like mesoporous structure consisting of amorphous pore walls. Taking these aspects into consideration, the roles of Zr- and Al-sites in different reaction steps were investigated for the two families of materials.

From the data in Table 4 for Fur conversion, a determinant effect of the Zr-sites on the one-pot process was clear. For each family of materials, the bio-products total yields tended to be higher for catalysts with lower ratio of Si/Zr, and the Zr-free catalysts led to sluggish Fur reaction. In comparison to the Zr-containing silicates, bulk ZrO_2 showed very poor catalytic activity, and led to comparable results to that without catalyst (19% and 9% conversion at 24 h, respectively). Taking into consideration the characterisation studies, the catalytic activity of the Zr-containing silicates may be due to isolated tetrahedral Zr species, which do not exist for (polymeric) ZrO_2. These results are in agreement with that reported by Corma and Renz [155], who demonstrated the ability of beta and MCM-41 type materials possessing isolated framework Zr-sites to promote CTH reactions of aldehydes to alcohols and the etherification of alcohols to the corresponding ether products. Moreover, computational studies reported in the literature have assessed the importance of tetrahedral Zr-sites of zeotypes for CTH reactions of carbonyl molecules with secondary alcohols as H-donors [62] and [156]. Thus, the tetrahedral Zr-sites seem to be essential for initialising the cascade process with the Fur reduction (step relative to k_1, Fig. 9).

The systematic studies of Zr-free and Zr-containing materials using FA, EMF and αAnL as substrates indicated that both Al- and Zr-sites of the silicates played roles as acid sites in these reactions. The Zr-sites of the silicates played roles in the CTH of Fur-FA, and also contributed, together with the Al-sites, to the acid-catalysed reactions. Bulk ZrO_2 was ineffective to convert the three substrates, indicating that its Zr-sites not only lack CTH activity as mentioned above, but also activity for the acid reactions. Interestingly, in the case of the model substrate EMF, the silicates exhibited transetherification activity, promoting its relatively fast conversion to 2BMF, 2BL, LA and AnLs (EL yield was less than 3% due to the favoured transetherification of EMF to 2BMF over the reaction of EMF to EL).

For each family of Zr-containing silicates with the substrates Fur, FA and FE, higher Al/Zr ratios (at similar ratio of Si/(Zr + Al)) tended to lead to favour the formation of 2BL, LA and AnLs (Fig. 7, Table 4). However, increasing Al/Zr had negative effects on the total yields of bio-products (Fig. 6 for Fur conversion). Hence, besides favouring the acid-catalysed steps leading to bio-products (e.g. steps relative to k_2, k_4 and k_5, Fig. 9), the Al-sites seemed to play roles in catalysing side-reactions.

With αAnL as substrate, the Zr-free and Zr-containing silicates led to 98–99% conversion after 7 h of reaction (Table 4) and the main bio-product was LA (61–72% yield after 7 h), besides 2BL (9–27% yield) and GVL (<1% yield). The LA yields were higher than the 2BL ones, whereas the opposite was observed for the Fur reaction in the presence of the Zr-containing catalysts. These results are consistent with the mechanistic proposal (*vide supra*) involving the conversion of FA to 2BL via parallel pathways (involving k_4 or k_5, Fig. 9).

The conversion of LA seems to be demanding in comparison to the other substrates (Table 4). The reaction starting from LA was in general slow, giving mainly 2BL. $(Zr)_{SSIE}$-beta led to the highest GVL yield of 22% at 56% LA conversion (2BL was formed with 10% yield), reached after 24 h of reaction. The Zr-containing TUD-1 type materials were poor catalysts for LA conversion (step relative to k_7, Fig. 9) and the same was observed for the conversion of the model substrate 1BL. The best-performing catalyst for 1BL conversion was $(Zr)_{SSIE}$-beta with 76% GVL yield at 83% conversion after 24 h (the other catalysts led to less than 10% GVL yield at 17–37% conversion, and bulk ZrO_2 was ineffective, Table 4).

For the modified beta materials, conversions of LA and 1BL, as well as GVL yields increased in the order $(ZrAl)_{SSIE}$-beta < $(Zr)_{SSIE}$-beta, which correlated with the decreasing ratios of Si/Zr and Al/Zr. This indicates that the Zr-sites played important roles in the CTH chemistry leading to GVL (k_8, Fig. 9). On the other hand, these results suggest that the Al-sites are not favourable for GVL formation. These results are in agreement with the literature for CTH reactions of cinnamaldehyde [87] and LA [70] in the presence of beta type materials, where the introduction of Al-sites into the zeolitic framework of Zr,Al-containing beta materials (prepared via hydrothermal synthesis) had a negative effect on the catalytic performance. The superior catalytic performance of $(Zr)_{SSIE}$-beta in the reactions of 1BL and LA correlates with its lower Si/Zr and Al/Zr ratios, and it is possible that this catalyst also possesses some Zr-sites with favourable intrinsic activity for GVL formation. According to the literature, the (tetrahedral) active Zr-sites may possess hydroxyl ligands which facilitate the formation of intermediate Zr-alkoxide transition states [62], [65], [68] and [156].

While $(Zr)_{SSIE}$-beta was effective in the reaction starting from the LE, it failed to produce GVL with high yields when Fur was the substrate. The systematic studies with LA and 1BL suggested that GVL was preferentially formed from the LE. However, the low LE yields for Fur conversion (9% at 7 h reaction) and for the other substrates (FA, EMF, αAnL and LA with less than 22% yield, Table 4) may have affected the (poor) GVL formation. Based on a literature overview for different steps leading to GVL (from LA [157], [158], [159] and [160], αAnL [58] or FA [161]), the low yields of 2BL in the present work may be due to limited acidity of the silicates prepared. Strong Brönsted heteropolyacids acids have been reported to promote the esterification of LA to LEs [157], [158], [159] and [160]; e.g. montmorillonite-supported dodecatungstophosphoric acid led to 100% 1BL selectivity at 97% LA conversion at 120 °C after 4 h [158]. In a patent application, Manzer [58] claimed much higher 1BL selectivity (99%) for the reaction of αAnL with 1-butanol, using Amberlyst™-15 (strong sulfonic acid ion-exchange resin) as catalyst in comparison to that of zeolite H-ZSM-5 (62%) at >96% conversion and 100 °C. A similar trend of zeolite H-beta versus Brönsted acid ion-exchange resins was reported by Lange et al. [161] for the conversion of FA to LEs in alcohol medium. Similarly, Carà et al. [49] reported higher activity of strong Brönsted

sulfonic acid functionalised mesoporous silicas than zeolites (H-ferrierite and H-ZSM-5) in FA conversion to 1BL. Hence, it can be concluded that strong Brönsted acidity favours formation of LEs, and the low GVL yields for the Zr-containing silicate catalysts of this work may be partly due to reduced acidity.

Finally, the multifunctionality of the Zr,Al-containing materials may be assessed as follows. For the beta type materials, it was demonstrated that their Zr-sites were essential for the CTH steps of Fur-FA, since their Zr-free synthesis precursor deAl-beta [46] was ineffective for catalysing this reaction step. On the other hand, the roles of the Al-sites of these catalysts were assessed by the fact that deAl-beta promoted the acid-catalysed reactions of FA, FE, and αAnL. It is worth emphasizing that $(Zr)_{SSIE}$-beta was prepared from deAl-beta by simply introducing Zr-sites and, consequently, the Si/Al ratios of the two materials are approximately equal (591 [46] and 588, respectively, Table 1). On the other hand, the type of Al-sites of deAl-beta [46] was essentially preserved in $(Zr)_{SSIE}$-beta (ascertained by the ^{27}Al MAS NMR spectroscopy). Hence, the contributions of the Al-sites of deAl-beta and $(Zr)_{SSIE}$-beta to the acid-catalysed steps may be considered equivalent. The Zr-sites also played roles in acid-catalysed reactions and thus the catalytic activity of $(Zr)_{SSIE}$-beta was generally higher than that of deAl-beta. Regarding the Zr,Al-containing TUD-1 type materials, these materials were effective for Fur reduction and increasing the amount of Al-sites favoured acid-catalysed steps. Overall, these results suggest that the Zr- and Al-sites of the silicate catalysts played effective roles in the one-pot catalytic process.

3.2.5. Kinetic modelling

Based on the overall Fur reaction mechanism represented in Fig. 9, a pseudo-homogeneous kinetic model was developed assuming perfectly stirred batch reactors, and first-order elementary reactions as in our recent work (described in Section 2.5) [46]. The one-pot system was modelled for the Zr-containing catalysts since the Zr-free ones were ineffective for Fur conversion. The kinetic model fitted reasonably well the experimental data (Fig. S10), with objective function (F obj) values in the range 7.49×10^{-4}–8.04×10^{-3} (Tables S1 and S2). Figs. S12 and S13 compare the k_i's for all steps and Zr-containing materials, and the values are given in Tables S1 and S2. The trends of the k_1 values (conversion of Fur) matched the experimentally observed Fur reaction rate, beta type catalysts being more active than the TUD-1 ones. For all catalysts, the fastest step was by far FA-2BMF (k_2), which is consistent with the high reactivity of the substrate FA as evident from the very low FA concentrations observed for the Fur system (Table 4). For the Zr-containing TUD-1 type catalysts, the kinetic constant of the FA-AnLs reaction step (k_3) was negligible; conversely, k_3 values for the modified beta catalysts were considerable (Fig. S12). These results are consistent with the higher AnLs yields reached for the beta type catalysts than the TUD-1 ones when Fur (Fig. 7b) as well as FA and FE were model substrates (Table 4). For each catalyst, a comparative study of the rate constants for the routes towards 2BL formation, i.e. 2BMF-AnLs-LA-2BL (k_4, k_6 and k_7) or 2BMF-2BL (k_5) indicated that the latter route is more favourable because the former route is strongly limited by the elementary step of LA-2BL (k_7, Fig. 9). These results are consistent with the relatively low reactivity of LA as discussed above (Table 4).

Fig. S14 shows the relationships between the k_i values for CTH and acid-catalysed reactions for each family of multifunctional Zr,Al-containing materials, and the results

are compared at similar Si/(Zr + Al) ratios. For each family of materials: (i) the kinetic constant associated with CTH activity, i.e. k_1 (Fur-FA, Fig. S14a and b) and k_8 (2BL-GVL, Fig. S14c and d), increased with decreasing ratios of Si/Zr and Al/Zr (i.e. increasing amount of Zr-sites); (ii) the kinetic constant for acid-catalysed steps (k_i values with i∈{3–7}) tended to increase with increasing Al/Zr (i.e. increasing amount of Al-sites); (iii) the kinetic constant of the parallel steps 2BMF-2BL (k_5) and 2BMF-AnLs (k_4) increased with increasing ratio of Al/Zr (Fig. S12), suggesting that the Al-sites promoted furan ring-opening reactions to give more end products; (iv) the kinetic constant associated with side-reactions (k_9–k_{14}) seemed more important for silicates with higher ratio Al/Zr (Fig. S13). These kinetic insights reveal the difficulty of optimising the relative amounts of Al- and Zr-sites of the multifunctional catalysts for converting Fur to more end bio-products such as GVL without favouring side reactions.

4. Conclusions

Porous Zr/Al-containing silicates of the type TUD-1 and zeolite beta with different Al/Zr ratios were prepared by relatively easy and eco-friendly methods. Spectroscopic characterisation of these silicates indicated that the Zr- and Al-sites were essentially in tetrahedral coordination (framework species) which accounted for catalyst multifunctionality. The silicates possessed catalytic activity and fairly good stability for the integrated reduction-acid reactions of Fur in 2-butanol, at 120 °C, leading to the bio-products 2BMF, 2BL, AnLs, LA (FA and GVL were formed in very small amounts), with total yields of up to 76% at 85% conversion. Systematic catalytic and kinetic studies coupled with characterisation studies for all silicates, helped establish relationships between the material and catalytic properties decisive for different steps of the overall reaction. The Zr-sites were essential for the reduction of Fur to FA, and LE to GVL; on the other hand, the Al- and Zr-sites played roles in intermediate acid-catalysed steps of FA conversion to 2BMF, 2BL, AnLs and LA. While (Zr)$_{SSIE}$-beta led to high GVL yields in the reaction starting from a levulinate ester substrate (77% at 83% 1BL conversion), it failed in leading to high GVL yields from Fur, which has been partly rationalised by the limited intermediate formation of the levulinate ester. These results suggested that a better compromise of acid properties was required. In this respect, multifunctional catalysts with higher Al/Zr ratios were prepared, which favoured the formation of the levulinate ester (and AnLs and LA), albeit these materials simultaneously promoted side-reactions. The challenges remain to develop eco-friendly heterogeneous multifunctional catalysts with optimum physicochemical properties for the efficient one-pot conversion of Fur to more end bio-products such as GVL.

Acknowledgements

SUPPLEMENTARY DATA
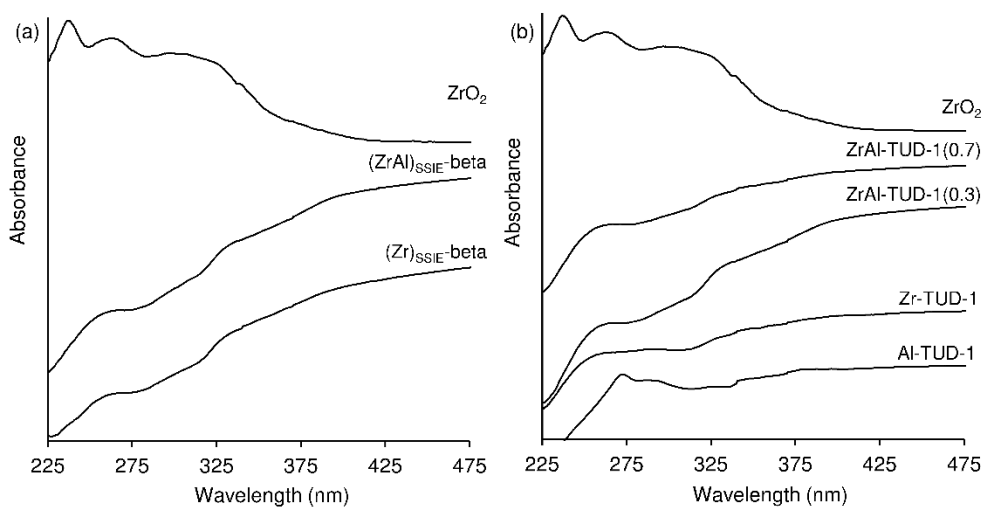
S.1. Characterisation data

Figure S1. Diffuse reflectance UV-vis spectra of (a) beta and (b) TUD-1 type materials; spectrum of bulk ZrO_2 is shown for comparison.
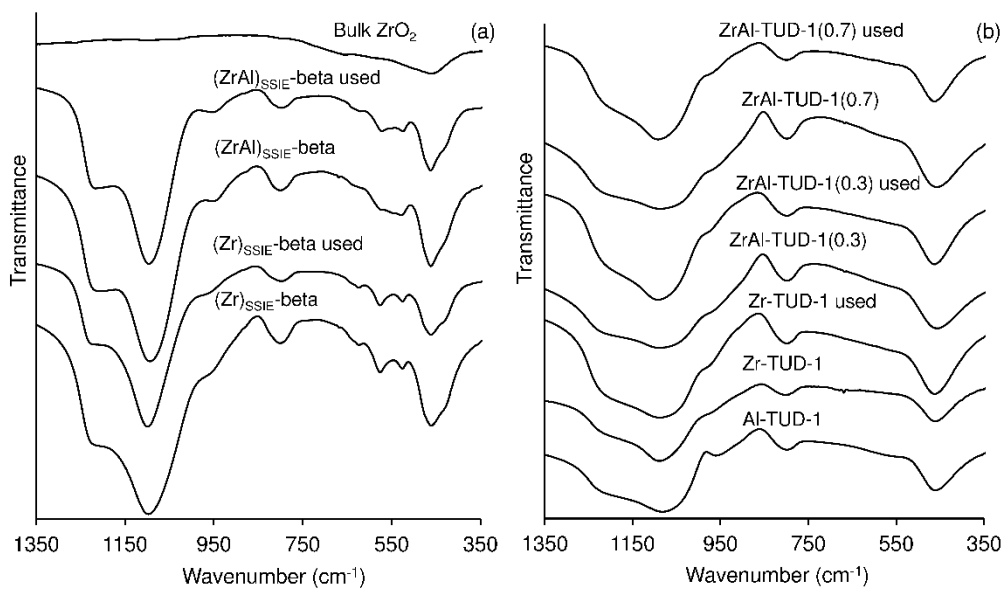

Figure S2. FT-IR ATR spectra of (a) modified beta materials and bulk ZrO_2, and (b) TUD-1 type materials.
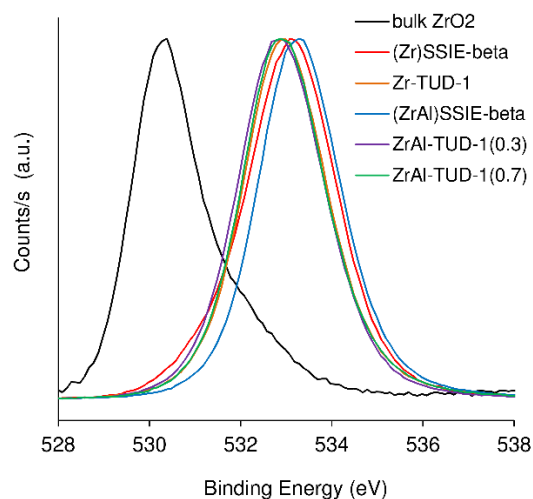
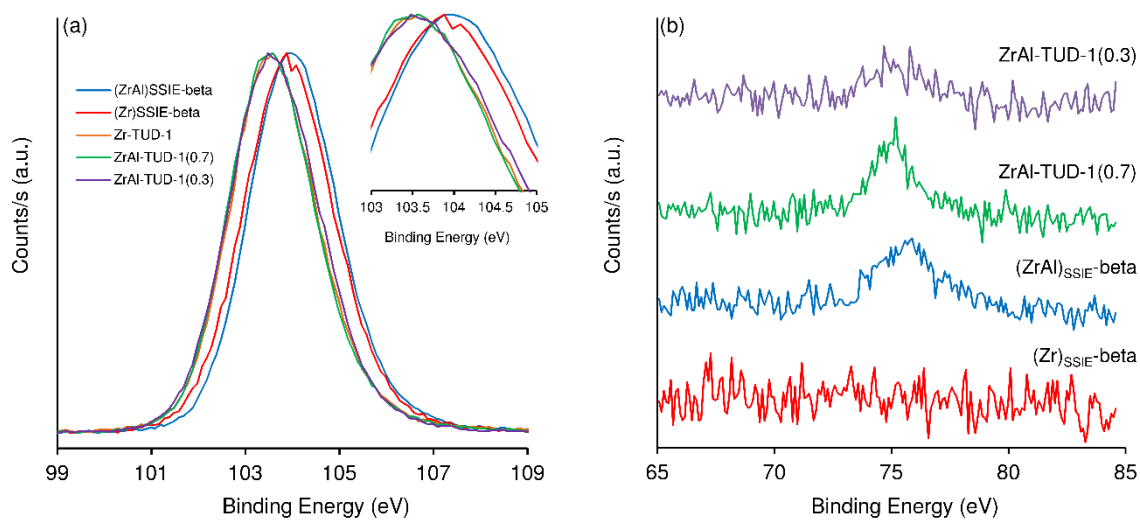**Figure S3.** O1s core level profiles of beta and TUD-1 type materials.

Figure S4. Si 2p (a) and Al 2p (b) core level spectra of beta and TUD-1 type materials; the colour legend is identical for (a) and (b). The inset in (a) is the expanded plot of the Si 2p core level spectra.
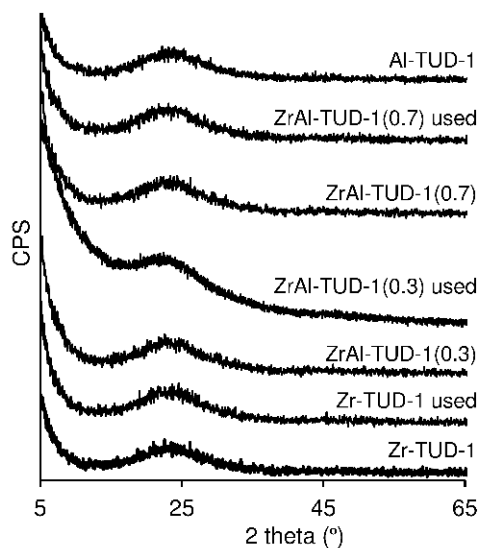
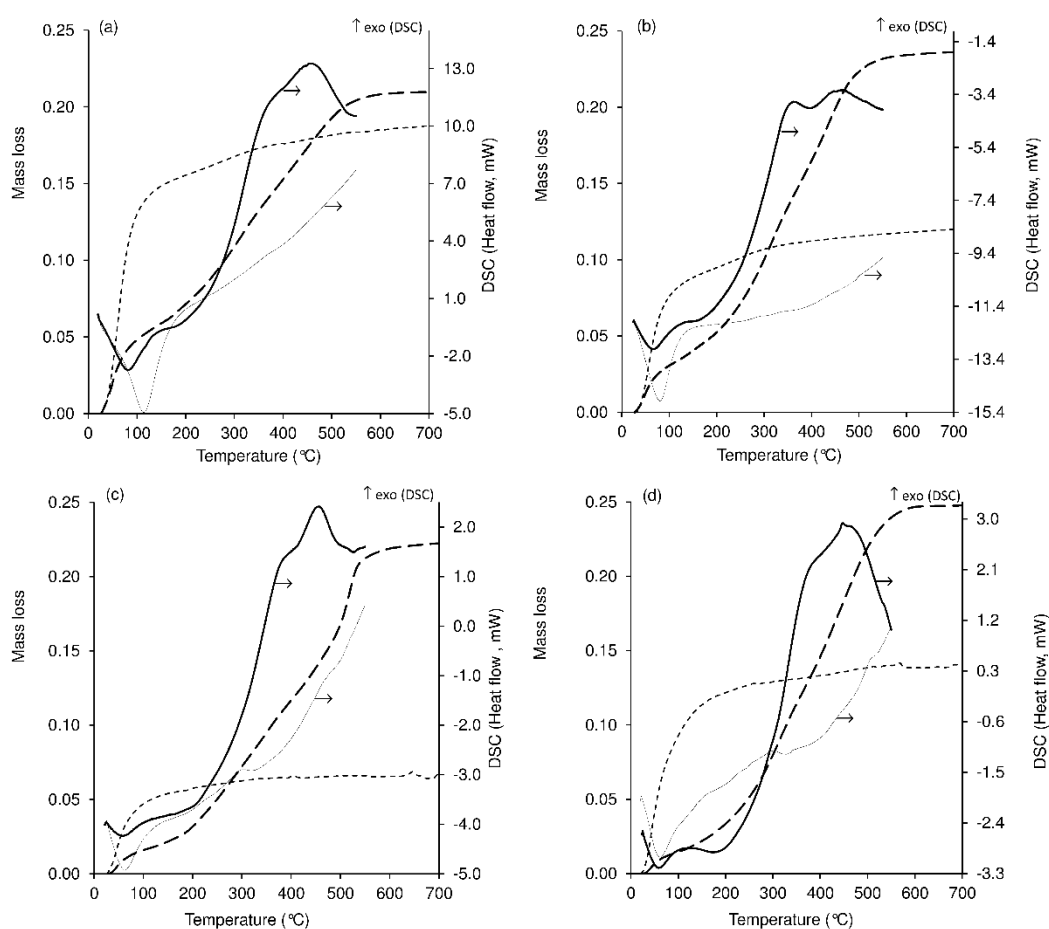**Figure S5.** High angle PXRD patterns of TUD-1 type materials.

Figure S6. TGA (mass loss fractions; dashes) and DSC (lines) analyses of Zr-TUD-1(a), ZrAl-TUD-1(0.7) (b), (Zr)$_{SSIE}$-beta (c), (ZrAl)$_{SSIE}$-beta (d) before (short dashes/thin lines) and after (long dashes/thick lines) a 24 h batch of Fur reaction.
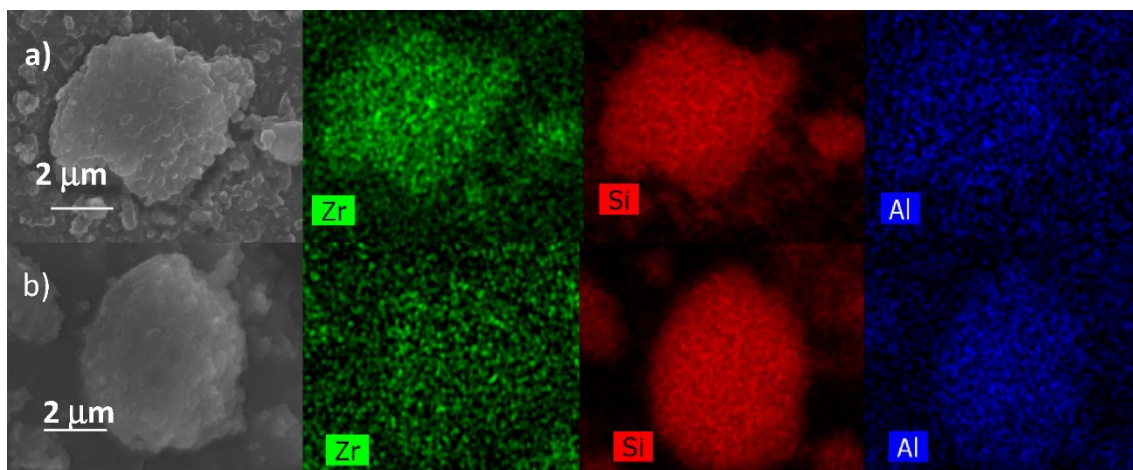

Figure S7. SEM and mapping of Al, Si and Zr for (Zr)$_{SSIE}$-beta (a) and (ZrAl)$_{SSIE}$-beta (b) recovered after the Fur reaction.
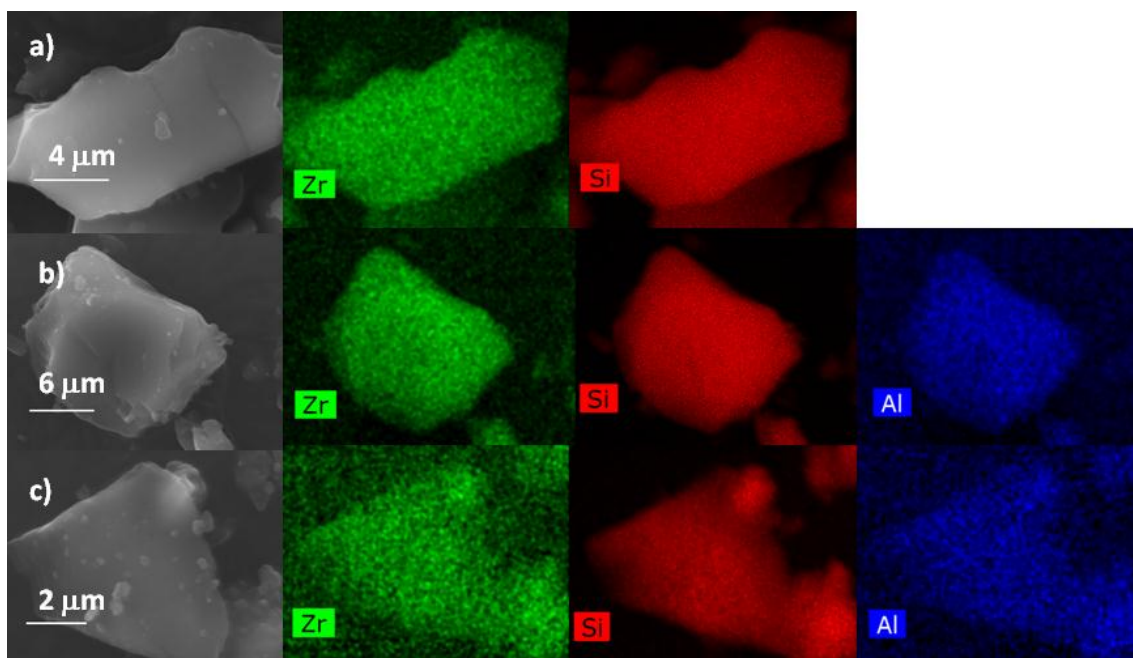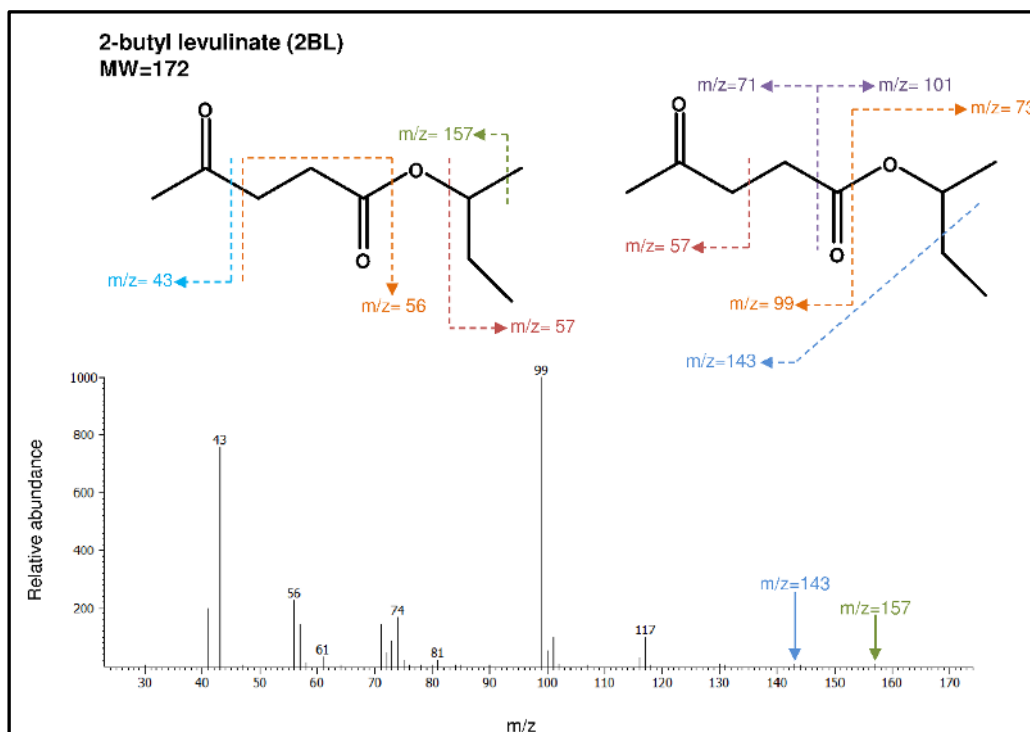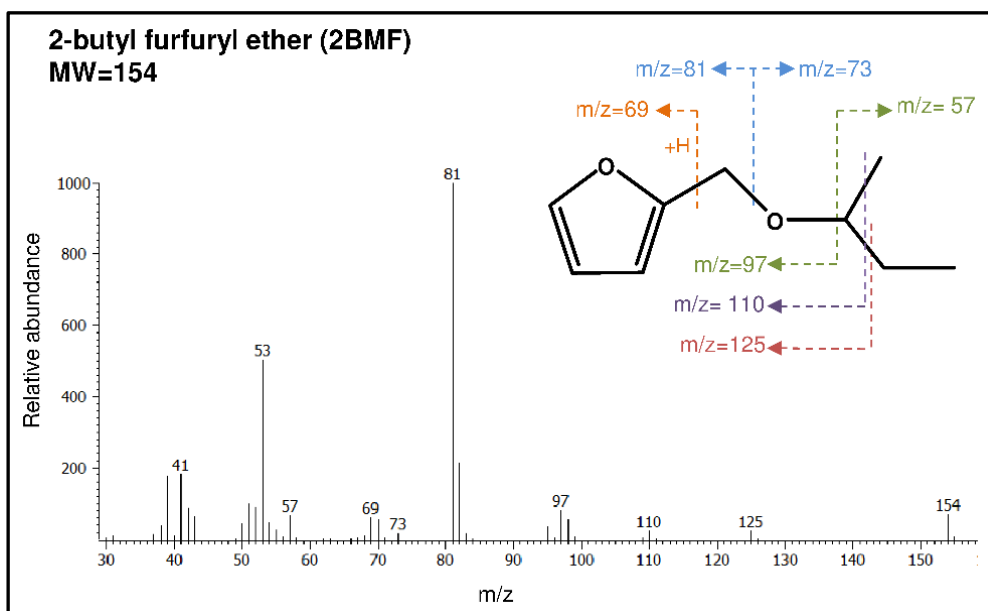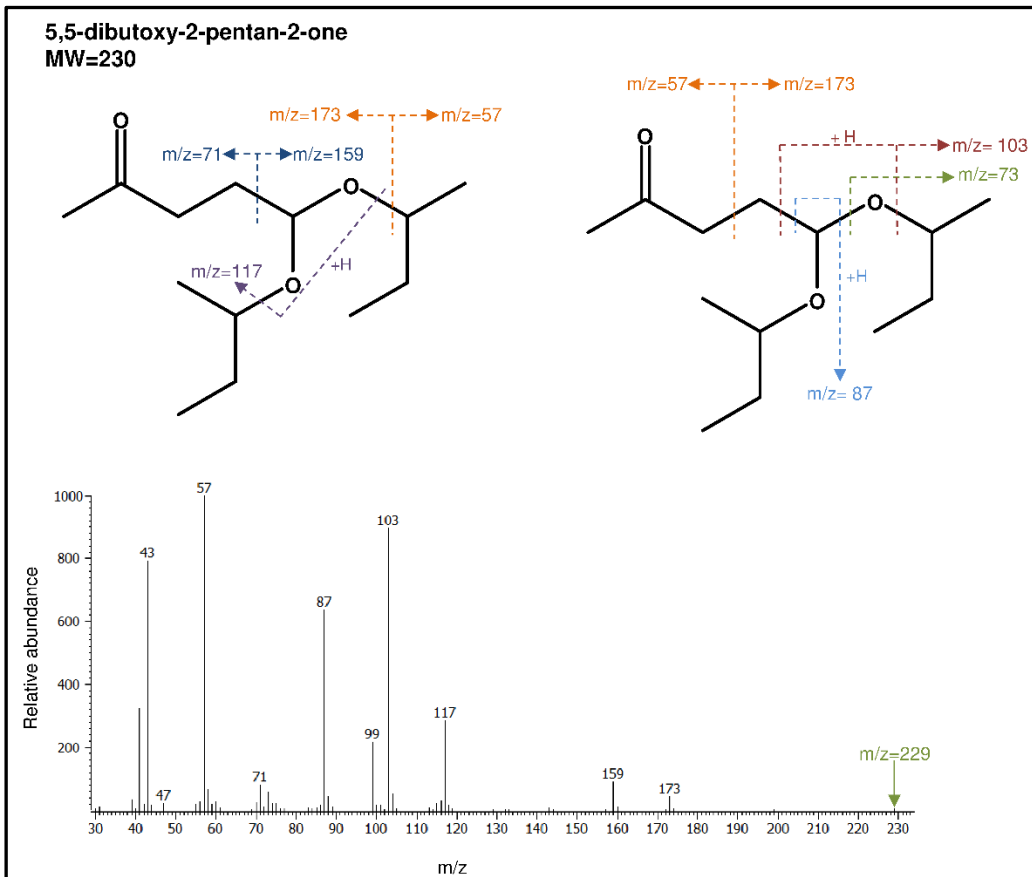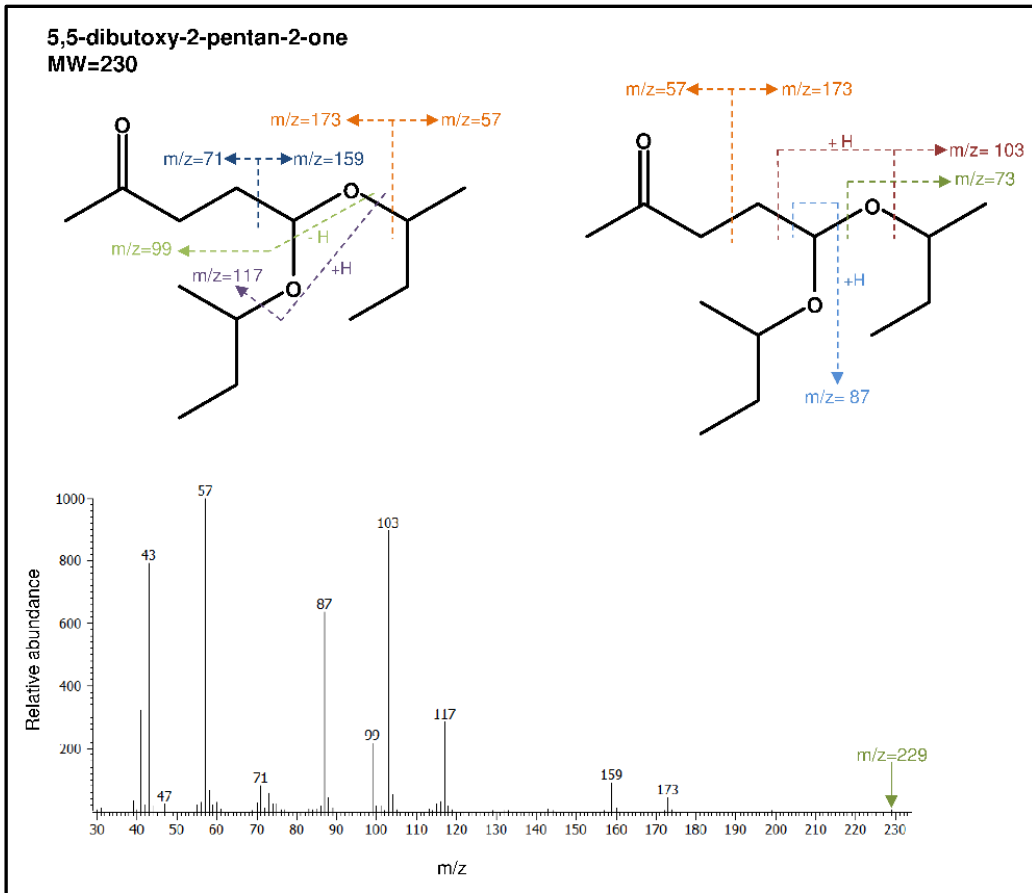

Figure S8. SEM and mapping of Al, Si and Zr for Al-TUD-1(a), Zr-TUD-1(b), ZrAl-TUD-1(0.3) (c) and ZrAl-TUD-1(0.7) (d) recovered after the Fur reaction.

S.2. Mass fragmentation patterns of bio-products and other products formed in the Fur reaction system

5,5-dibutoxy-2-pentan-2-one
MW=230

5,5-dibutoxy-2-pentan-2-one
MW=230

S.3. Kinetic model

The micro reactors were modelled as perfectly stirred batch reactors, and the mass balance equations are given by:

$$\frac{V}{W}\frac{dC_i}{dt} = r_i$$

Eq. (1)

where V is the reaction mixture volume (L), W is the mass of catalyst (g), C_i is the molar concentration of the reactive species i (M), t is time (h), and r_i is the overall reaction rate of species i expressed per unit of mass catalyst (mol·g_{cat}^{-1}·h^{-1}). The ratio W/V was maintained constant in all experiments.

Based on the mechanism proposed in Scheme S1 a pseudo-homogeneous kinetic model was developed, considering first-order reactions for all steps involved. Possible loss-reactions of the species involved were considered, since, in general, the mole balances did not close for different bio-products as substrates (D_m denotes by-products formed from species m, and m is Fur, 2BMF, AnLs, LA, 2BL or GVL).

$$\frac{V}{W}\frac{dC_{FUR}}{dt} = -\left(k_1 + k_9\right)C_{FUR}$$

Eq. (2)

$$\frac{V}{W}\frac{dC_{FA}}{dt} = k_1\,C_{FUR} - \left(k_2 + k_3 + k_{10}\right)C_{FA}$$

Eq. (3)

$$\frac{V}{W}\frac{dC_{2BMF}}{dt} = k_2\,C_{FA} - \left(k_4 + k_5 + k_{11}\right)C_{2BMF}$$

Eq. (4)

$$\frac{V}{W}\frac{dC_{AnLs}}{dt} = k_3\,C_{FA} + k_4\,C_{2BMF} - \left(k_6 + k_{12}\right)C_{AnLs}$$

Eq. (5)

$$\frac{V}{W}\frac{dC_{LA}}{dt} = k_6\,C_{AnLs} - \left(k_7 + k_{13}\right)C_{LA}$$

Eq. (6)

$$\frac{V}{W}\frac{dC_{2BL}}{dt} = k_5\,C_{2BMF} + k_7\,C_{LA} - \left(k_8 + k_{14}\right)C_{2BL} \qquad\qquad \text{Eq. (7)}$$

$$\frac{V}{W}\frac{dC_{GVL}}{dt} = k_8\,C_{2BL} \qquad\qquad \text{Eq. (8)}$$

$$\frac{V}{W}\frac{dC_{D_{Fur}}}{dt} = k_9\,C_{Fur} \qquad\qquad \text{Eq. (9)}$$

$$\frac{V}{W}\frac{dC_{D_{FA}}}{dt} = k_{10}\,C_{FA} \qquad\qquad \text{Eq. (10)}$$
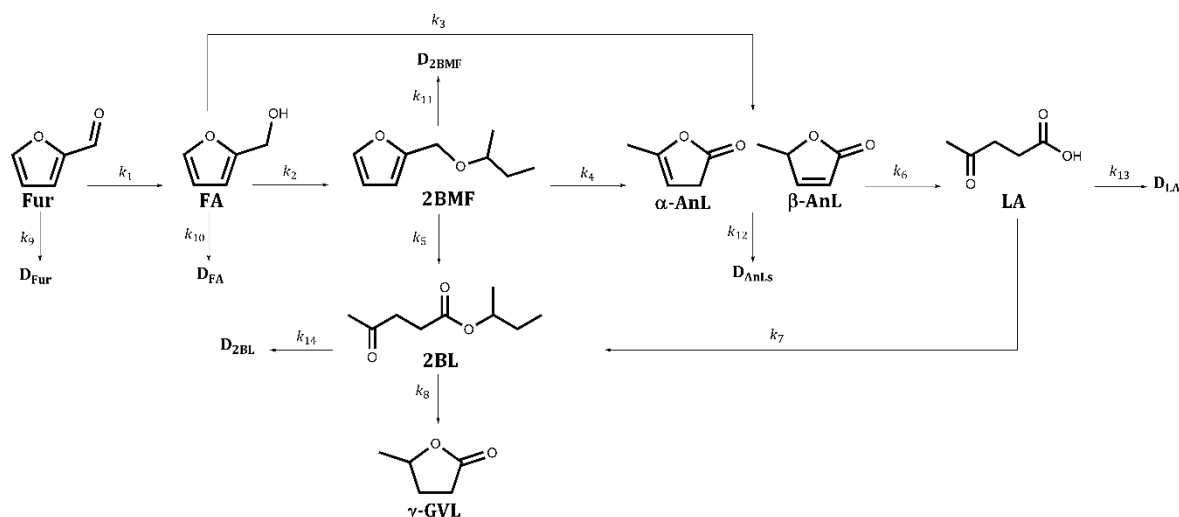
$$\frac{V}{W}\frac{dC_{D_{2BMF}}}{dt} = k_{11}\,C_{2BMF} \qquad\qquad \text{Eq. (11)}$$

$$\frac{V}{W}\frac{dC_{D_{AnLs}}}{dt} = k_{12}\,C_{AnLs} \qquad\qquad \text{Eq. (12)}$$

$$\frac{V}{W}\frac{dC_{D_{LA}}}{dt} = k_{13}\,C_{LA} \qquad\qquad \text{Eq. (13)}$$

$$\frac{V}{W}\frac{dC_{D_{2BL}}}{dt} = k_{14}\,C_{2BL} \qquad\qquad \text{Eq. (14)}$$

where k_j are the apparent reaction kinetic constants ($L \cdot g_{cat}^{-1} \cdot h^{-1}$) of step j at constant

temperature.

Scheme S1. Mechanistic proposal for the overall Fur conversion (adapted from ref.[1]).

The problem was solved by numerical integration with simultaneous optimisation, using appropriate initial conditions (at t=0). MEIGO (Metaheuristics for systems biology and bIoinformatics Global Optimization) [2] an open-source toolbox for global optimisation, and Matlab® (version 7.8) were used to obtain the kinetic constants by fitting the model proposed to the experimental data (up to 7h) in order to minimise the following objective function:

$$F_{\text{obj}} = \sum_m \left\{ \sum_{n=1}^{n_{\text{p}}} \left[C_{m,n}\big|_{\text{calc}} - C_{m,n}\big|_{\text{exp}} \right]^2 \right\} \qquad \text{Eq. (14)}$$

where $C_{m,n}\big|_{\text{calc}}$ and $C_{m,n}\big|_{\text{exp}}$ are the concentrations predicted by the model and the experimental ones, respectively, at each instant of time n.

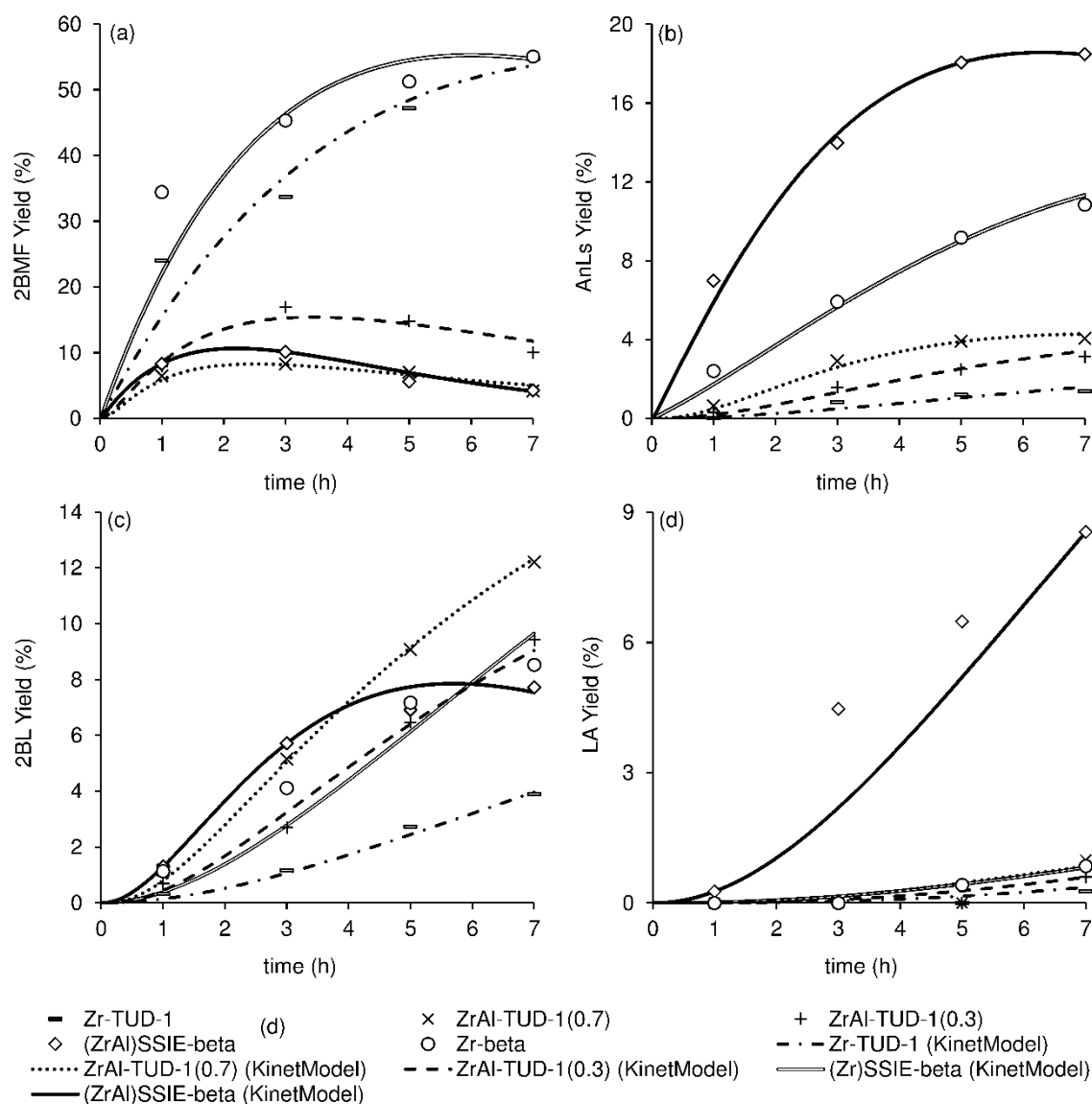## S.4. Catalytic and kinetic modelling results

Figure S9. Dependence of the yields of 2BMF (a), AnLs (b), 2BL (c) and LA (d) on Fur reaction time, in the presence of Zr-TUD-1 (-), ZrAl-TUD-1(0.3) (+), ZrAl-TUD-1(0.7) (×), (Zr)$_{SSIE}$-beta (o) or (ZrAl)$_{SSIE}$-beta (◊), at 120 °C. The lines correspond to the curves calculated by kinetic modelling (KinetModel).
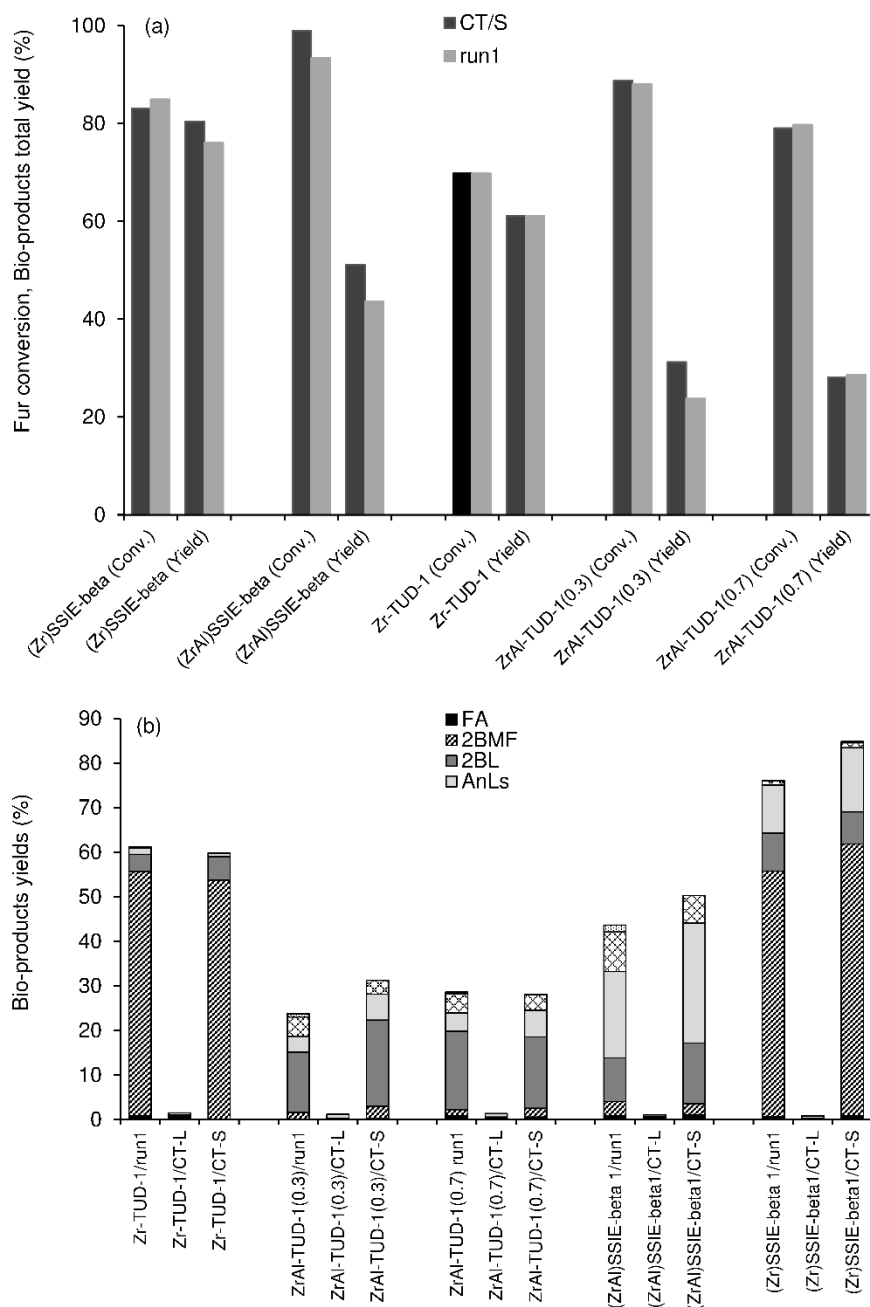
Figure S10. Catalytic results for the Zr-containing silicates tested in the Fur reaction with 2BuOH, at 120 ℃ (run 1), and for corresponding solid (CT-S) and liquid phases (CT-L) obtained from the contact tests (CT).
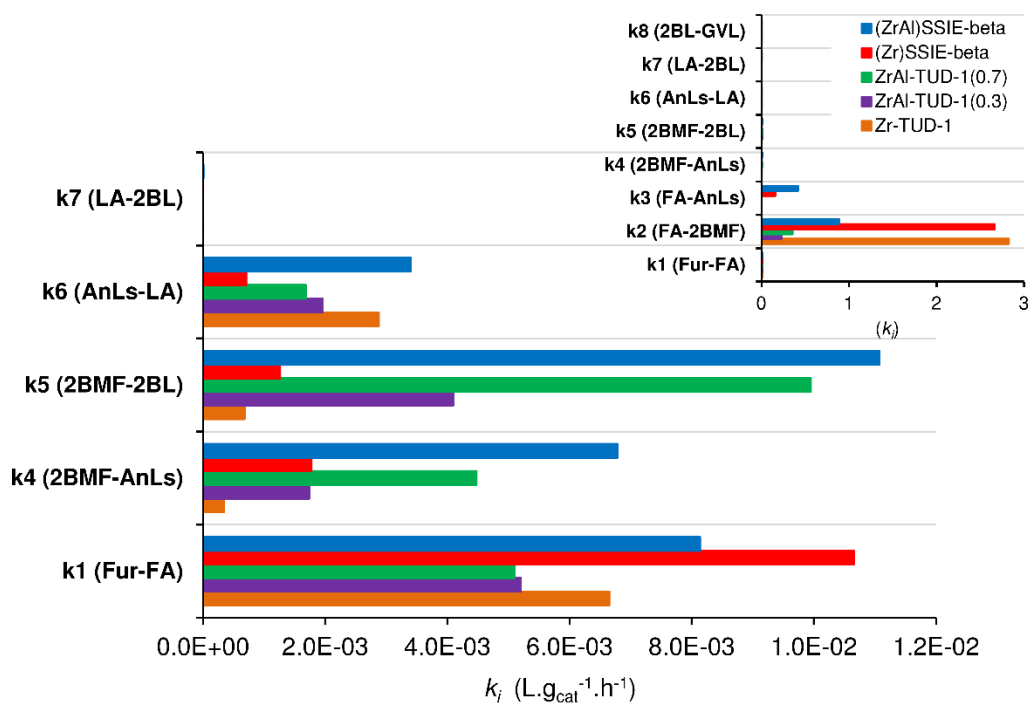
Figure S11. Modelled rate constants (k_i) for the conversion of Fur to the bio-products in the presence of the Zr-containing silicate catalysts. The inset compares k_1 to k_8, and the smaller k_i values are compared in the figure on the left. The colour legend given in the inset is the same for the two bar charts. The k_i values are given in Tables S1 and S2.

Figure S12. Modelled rate constants (k_i) for the steps of non-productive consumption of bio-products. The k_i values are given in Tables S1 and S2.

Table S1. Kinetic constants (k_j), confidence intervals at 90% and parameter error (%), of the modelled overall reaction of Fur, in the presence of $(Zr)_{SSIE}$-beta or $(ZrAl)_{SSIE}$-beta in 2-butanol, at 120 ℃.
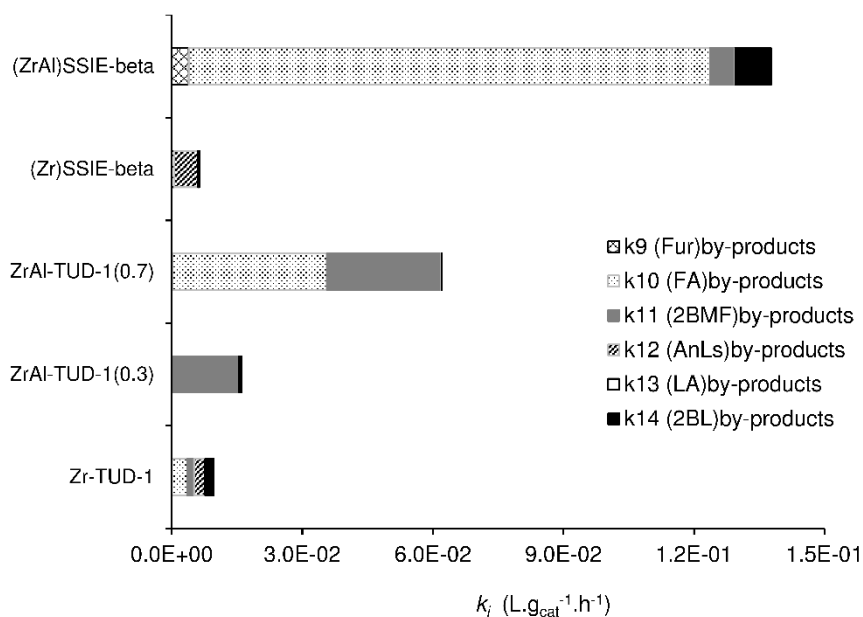
Rate constant ($L \cdot g_{cat}^{-1}, h^{-1}$)	$(Zr)_{SSIE}$-beta	Error (%)	$(ZrAl)_{SSIE}$-beta	Error (%)
$k_1 \pm \Delta k_1$	$(1.065 \pm 0.012) \times 10^{-2}$	1.08	$(8.132 \pm 0.631) \times 10^{-3}$	7.76
$k_2 \pm \Delta k_2$	2.660 ± 0.269	10.10	$(8.832 \pm 1.123) \times 10^{-1}$	12.72
$k_3 \pm \Delta k_3$	$(1.534 \pm 0.128) \times 10^{-1}$	8.35	$(4.153 \pm 0.520) \times 10^{-1}$	12.52
$k_4 \pm \Delta k_4$	$(1.774 \pm 0.035) \times 10^{-3}$	2.00	$(6.785 \pm 0.617) \times 10^{-3}$	9.09
$k_5 \pm \Delta k_5$	$(1.262 \pm 0.027) \times 10^{-3}$	2.11	$(1.107 \pm 0.080) \times 10^{-2}$	7.19
$k_6 \pm \Delta k_6$	$(7.036 \pm 0.816) \times 10^{-4}$	11.59	$(3.398 \pm 0.202) \times 10^{-3}$	5.94
$k_7 \pm \Delta k_7$	$(3.704 \pm 0.223) \times 10^{-6}$	6.03	$(5.625 \pm 0.947) \times 10^{-6}$	16.83
$k_8 \pm \Delta k_8$	$(2.293 \pm 0.294) \times 10^{-4}$	12.82	$(1.167 \pm 0.116) \times 10^{-4}$	9.95
$k_9 \pm \Delta k_9$	$(5.637 \pm 0.094) \times 10^{-4}$	1.66	$(3.924 \pm 0.470) \times 10^{-3}$	11.98
$k_{10} \pm \Delta k_{10}$	–	–	$(1.198 \pm 0.141) \times 10^{-1}$	11.77
$k_{11} \pm \Delta k_{11}$	–	–	$(5.739 \pm 0.717) \times 10^{-3}$	12.49
$k_{12} \pm \Delta k_{12}$	$(5.531 \pm 0.461) \times 10^{-3}$	8.34	$(1.002 \pm 0.143) \times 10^{-4}$	14.26
$k_{13} \pm \Delta k_{13}$	–	–	$(1.062 \pm 0.099) \times 10^{-5}$	9.36
$k_{14} \pm \Delta k_{14}$	$(2.264 \pm 0.283) \times 10^{-4}$	12.48	$(8.096 \pm 0.673) \times 10^{-3}$	8.31
F_{obj} (M^2)	8.04×10^{-3}		8.79×10^{-4}	

[a] The error associated to each kinetic rate constant is given by $(\Delta k_i / k_i) \times 100$; [b] The objective function was the sum of squared deviations:

$$F_{obj} = \sum_m \left\{ \sum_{n=1}^{n_p} \left[C_{m,n} \big|_{calc} - C_{m,n} \big|_{exp} \right]^2 \right\},$$ where $C_{m,n}\big|_{calc}$ and $C_{m,n}\big|_{exp}$ are the calculated and experimental concentrations of specie m (Fur, Fur, 2BMF, AnLs, LA, 2BL and GVL), respectively, at reaction time n.

Table S2. Kinetic constants (k_j), confidence intervals at 90% and parameter error (%), of the modelled overall reaction of Fur, in the presence of Zr-TUD-1, ZrAl-TUD-1(0.3) or ZrAl-TUD-1(0.7) in 2-butanol, at 120 ºC.

Rate constant ($L·g_{cat}^{-1}, h^{-1}$)	Zr-TUD-1	Error (%)	ZrAl-TUD-1(0.3)	Error (%)	ZrAl-TUD-1(0.7)	Error (%)
$k_1 \pm \Delta k_1$	$(6.647 \pm 0.072) \times 10^{-3}$	1.08	$(5.197 \pm 0.129) \times 10^{-3}$	2.49	$(5.099 \pm 0.171) \times 10^{-3}$	3.36
$k_2 \pm \Delta k_2$	2.823 ± 0.081	2.86	$(2.249 \pm 0.099) \times 10^{-1}$	4.38	$(3.516 \pm 0.329) \times 10^{-1}$	9.36
$k_3 \pm \Delta k_3$	–	–	–	–	–	–
$k_4 \pm \Delta k_4$	$(3.394 \pm 0.202) \times 10^{-4}$	5.94	$(1.738 \pm 0.138) \times 10^{-3}$	7.93	$(4.472 \pm 0.229) \times 10^{-3}$	5.12
$k_5 \pm \Delta k_5$	$(6.788 \pm 0.179) \times 10^{-4}$	2.63	$(4.093 \pm 0.102) \times 10^{-3}$	2.49	$(9.948 \pm 0.666) \times 10^{-3}$	6.70
$k_6 \pm \Delta k_6$	$(2.874 \pm 0.059) \times 10^{-3}$	2.05	$(1.955 \pm 0.174) \times 10^{-3}$	8.88	$(1.680 \pm 0.125) \times 10^{-3}$	7.46
$k_7 \pm \Delta k_7$	$(2.152 \pm 0.419) \times 10^{-7}$	19.45	–	–	–	–
$k_8 \pm \Delta k_8$	$(8.590 \pm 0.830) \times 10^{-5}$	9.67	$(1.169 \pm 0.117) \times 10^{-4}$	10.02	$(3.645 \pm 0.100) \times 10^{-5}$	2.75
$k_9 \pm \Delta k_9$	$(5.004 \pm 0.433) \times 10^{-7}$	8.65	$(5.363 \pm 0.510) \times 10^{-5}$	9.51	$(1.794 \pm 0.228) \times 10^{-4}$	12.71
$k_{10} \pm \Delta k_{10}$	$(3.552 \pm 0.171) \times 10^{-3}$	4.82	–	–	$(3.545 \pm 0.346) \times 10^{-2}$	9.76
$k_{11} \pm \Delta k_{11}$	$(1.551 \pm 0.018) \times 10^{-3}$	1.19	$(1.550 \pm 0.096) \times 10^{-2}$	6.19	$(2.615 \pm 0.350) \times 10^{-2}$	13.40
$k_{12} \pm \Delta k_{12}$	$(2.576 \pm 0.055) \times 10^{-3}$	2.12	$(1.244 \pm 0.186) \times 10^{-6}$	14.96	$(1.881 \pm 0.329) \times 10^{-4}$	17.48
$k_{13} \pm \Delta k_{13}$	–	–	–	–	–	–
$k_{14} \pm \Delta k_{14}$	$(1.951 \pm 0.083) \times 10^{-3}$	4.26	$(4.255 \pm 0.459) \times 10^{-4}$	10.80	$(7.508 \pm 0.731) \times 10^{-5}$	9.74
$F_{obj} (M^2)$	4.54×10^{-3}		9.81×10^{-4}		7.49×10^{-4}	

Note: [a] and [b] are the same presented in Table S1.

References

1. M. M. Antunes, S. Lima, P. Neves, A. L. Magalhães, E. Fazio, A. Fernandes, F. Neri, C. M. Silva, S. M. Rocha, M. F. Ribeiro, M. Pillinger, A. Urakawa , A. A. Valente, J. Catal. (2015), doi: 10.1016/j.jcat.2015.1005.1022.

2. J. A. Egea, D. Henriques, T. Cokelaer, A. F. Villaverde, A. MacNamara, D.-P. Danciu, J. R. Banga , J. Saez-Rodriguez, BMC Bioinformatics 15 (2014) 136-144.

References

1. M. M. Antunes, S. Lima, P. Neves, A. L. Magalhães, E. Fazio, A. Fernandes, F. Neri, C. M. Silva, S. M. Rocha, M. F. Ribeiro, M. Pillinger, A. Urakawa , A. A. Valente, J. Catal. (2015), doi: 10.1016/j.jcat.2015.1005.1022.

2. J. A. Egea, D. Henriques, T. Cokelaer, A. F. Villaverde, A. MacNamara, D.-P. Danciu, J. R. Banga , J. Saez-Rodriguez, BMC Bioinformatics 15 (2014) 136-144.